IEEE Access
Multidisciplinary ⋮ Rapid Review ⋮ Open Access Journal

Received January 18, 2020, accepted February 1, 2020, date of publication February 10, 2020, date of current version February 19, 2020.

Digital Object Identifier 10.1109/ACCESS.2020.2972947

Stability and Suppression Study for Low-Frequency Oscillations in Network-Train System

SHAOBING YANG[1], (Member, IEEE), YINGCHEN WANG[1], KEJIAN SONG[1], (Member, IEEE), MINGLI WU[1], (Member, IEEE), AND GEORGIOS KONSTANTINOU[2], (Senior Member, IEEE)

[1]School of Electrical Engineering, Beijing Jiaotong University, Beijing 100044, China
[2]School of Electrical Engineering and Telecommunications, University of New South Wales, Sydney, NSW 2052, Australia

Corresponding author: Kejian Song (songkj@bjtu.edu.cn)

This work was supported in part by the National Key Research and Development Program of China under Grant 2017YFB1200802, and in part by the National Postdoctoral Program for Innovative Talents under Project BX201700026.

ABSTRACT Electric multiple units (EMUs) have been the cause of low frequency oscillation (LFO) incidents in high-speed railway (HSR) network train systems (NTSs). In this paper a norm criterion with the advantages of simpler calculation while being less conservative than other norm criteria is introduced to analyze the stability of the NTS. A control strategy of EMU four-quadrant converters (4QCs) consisting of ac current passivity-based control (PBC) and dc voltage sliding mode variable structure (SMS) control, i.e. PBC-SMS, is proposed for LFO suppression. The NTS stability analysis with PBC-SMS results in superior critical LFO condition. A single EMU simulation validates the improved steady-state and dynamic performance of the PBC-SMS compared to other conventional methods; NTS simulations based on field tested network parameters verify the superior LFO suppression capability of the proposed method. Finally, guidelines for LFO suppression are recommended based on a comprehensive sensitivity analysis of the traction network, 4QC circuit and controller parameters of an NTS.

INDEX TERMS High-speed railways, low-frequency oscillation, network-train system, passivity-based control, sliding mode variable structure, stability analysis, sensitivity analysis.

I. INTRODUCTION

WITH the rapid development of high-speed railways (HSRs), large numbers of electric multiple units (EMUs) have been put into operation. Since each EMU train uses a number of interleaved four-quadrant converters (4QCs) as front-end rectifiers to draw power from the traction network [1], [2], many power electronic converters are connected to traction power supply systems (TPSSs), resulting in low-frequency oscillation (LFO) incidents in different traction supplies (ac 25 kV, ac 15 kV, etc.) worldwide. A first LFO incident occurred in Norwegian railways in 1996 [3], while similar problems occurred successively in France, USA, Germany, and Switzerland [4], [5]. In recent years, LFO instances have caused some traction blockades of EMUs in China, delaying departures and even affecting the stable and safe operation of railways [6].

Generally, when there is a mismatch between the parameters of the EMU 4QCs and supply network, the network-train system (NTS) may be unstable, leading to LFOs [7]. Previous studies analyzed the LFO mechanism through stability studies on the NTS [8]–[12]. Based on the equivalent impedance/ admittance models of the network and train, a range of stability criteria, such as the generalized Nyquist criterion [8], dominant pole [9], norm criterion [10] and forbidden region-based criterion [11], [12] were used. In [8], the disadvantages of the Nyquist criterion in LFO analysis and an alternative method based on Bode diagrams were presented. Dominant poles were used to analyze the variation law of equivalent train impedance with respect to 4QCs control parameters when a LFO occurred [9], resulting in an optimal order for adjusting the control parameters. Using the norm criterion, the NTS stability ensuring safe margin, were presented in [10]. Refs. [11] and [12] investigated the stability of multiple trains entering a supply section, revealing the negative impedance nature of 4QCs during LFO instances.

LFOs can be suppressed by improving the stability of 4QCs control, for example through nonlinear auto-disturbance rejection control (ADRC) [13] and adaptive ADRC [14]. By adjusting the gains of the conventional PI control, the

The associate editor coordinating the review of this manuscript and approving it for publication was Wei Wei.

anti-disturbance capability of the controllers is increased, reducing the chances of LFO occurring in the system, but at the cost of reduced dynamics. Some advanced controllers consider both system stability and dynamic performance [15]–[20]. The model predictive direct power control (MPDPC) of [15] achieves LFO suppression with good dynamic performance but is sensitive to the parameters of the model. An extended state observer (ESO) is incorporated with model predictive control (MPC) to improve parameter sensitivity [16]. During transients, the "ESO+MPC" scheme offers fast response but large dc voltage overshoots are observed. The large number of parameters that require tuning is another issue with the method. The H∞ method of [17] reduces overshoot but increases the steady-state dc voltage ripple. An LFO suppression method based on passivity-based control (PBC) was proposed in [18] reducing both overshoot and dc voltage ripple, again at the cost of dynamic response. A nonlinear PBC controller is designed for the single-phase rectifier in [19], which can optimize the load characteristics and suppress the LFO. Sliding mode variable structure (SMS) can also suppress LFOs with fast dynamic response and small dc voltage overshoot [20]. However, the large dc voltage ripple under steady state and its sensitivity to model parameters [21] require the combination of the SMS with other methods, such as observers, adaptive control etc.

Based on the previous analysis, the following gaps are identified in the literature:

1) There is no control method for LFO suppression that considers the steady-state, dynamic performance and robustness without extensive requirements in parameter tuning.
2) There is no quantitative investigation and stability analysis for advanced control methods (i.e. adaptive ADRC, MPDPC, ESO+MPC, H∞, PBC, SMS, etc.).
3) The impact of variations in the network and 4QC controller parameters in the system stability under advanced control have not been discussed in depth.

In order to fill up the deficiencies of previous work with regards to the LFO suppression, this paper proposes an EMU 4QC control strategy for LFO suppression based on ac current PBC and dc voltage SMS (named PBC-SMS). The main contributions and technical novelty of the work are as follows:

1) The proposed PBC-SMS controller for LFO suppression demonstrates good steady-state and dynamic performance with fewer control parameters, exhibiting strong robustness to system parameter deviation and external disturbance.
2) A stability analysis based on norm criterion is applied to the NTS for both the conventional and proposed control methods, indicating their LFO critical conditions.
3) The impact of traction network, 4QC circuit and controller parameters on the NTS stability is comprehensively investigated, resulting in a number of recommendations for avoiding LFO incidents.

The rest of this paper is organized as follows. In Section II, an LFO incident is described as a typical study case.

TABLE 1. LFO cases in china electric railways.

Vehicle		f_{LFO} (Hz)	Occurrence time	Location
Type	N_{Cri}			
HX_D1	6	3-4	Jan. 2008	Daqin Hudong
CRH1	11	5	Jan. 2010	Shanghai Nanxiang
CRH5	6	5	Sept. 2010	Qingdao
HX_D2B	-	5	Jun. 2011	Xuzhou
HX_D3B	9	6-7	Nov. 2011	Shanhaiguan
HX_D2B	-	2	Jan. 2014	North of Xuzhou

Note: N_{Cri} means the critical number of EMUs/locomotives for LFO; f_{LFO} is the LFO frequency.

The NTS is then modeled in the dq frame and stability analysis based on a norm criterion method is performed. The PBC-SMS control of 4QC is proposed in Section III. Stability study of the NTS with the proposed controller is carried out in Section IV. In Section V, single EMU and entire system simulations validate that the proposed controller has superior LFO suppression capability with better steady-state and dynamic performance compared to more conventional methods. The impact of system parameters on the stability is investigated in Section VI where four recommendations for LFO suppression is obtained. Section VII draws conclusion for this work.

II. MECHANISM ANALYSIS OF LFO IN NTS

A. A TYPICAL LFO CASE

From 10 to 16 September 2010, LFOs frequently occurred in the Qingdao EMU operation depot due to the large number of CRH5 EMUs in operation, leading to traction blockades of the EMUs. During the LFO incident, all the operation EMUs in the depot were under light load, and the stability issue of the NTS is more likely to occur under this condition than the heavy load [6]. The field test results of this incident are shown in Fig. 1.

As shown in Fig. 1(a), when 5 EMUs were put into operation synchronously, the measured 4QC ac side voltage and current exhibited slight oscillations, while the dc link voltage, supply voltage and traction network current did not show obvious oscillations. However, as shown in Fig. 1(b), when 6 EMUs were put into operation simultaneously, a 5 Hz oscillation appeared in all electrical quantities of the 4QC and network sides, indicating instability in the NTS.

Typical LFO incidents occurred in China are summarized in TABLE 1 [4], illustrating that i) different EMUs (CRH series)/locomotives (HX_D series) may excite LFOs of different frequencies (2-7 Hz for Chinese cases), and ii) the occurrence of an LFO is closely related to the number of EMUs/locomotives operating under the same supply.

B. SYSTEM MODELING BY RETURN-RATIO MATRIX

An NTS can be depicted as a cascaded structure as shown in Fig. 2. Although this is a multiple input and multiple output (MIMO) system, it can be simply seen as a "source-load" model [9]. The source, i.e. the traction network, is represented by an equivalent Thévenin circuit; the load, i.e. multiple EMUs, can be modeled by connecting the EMU input admit-

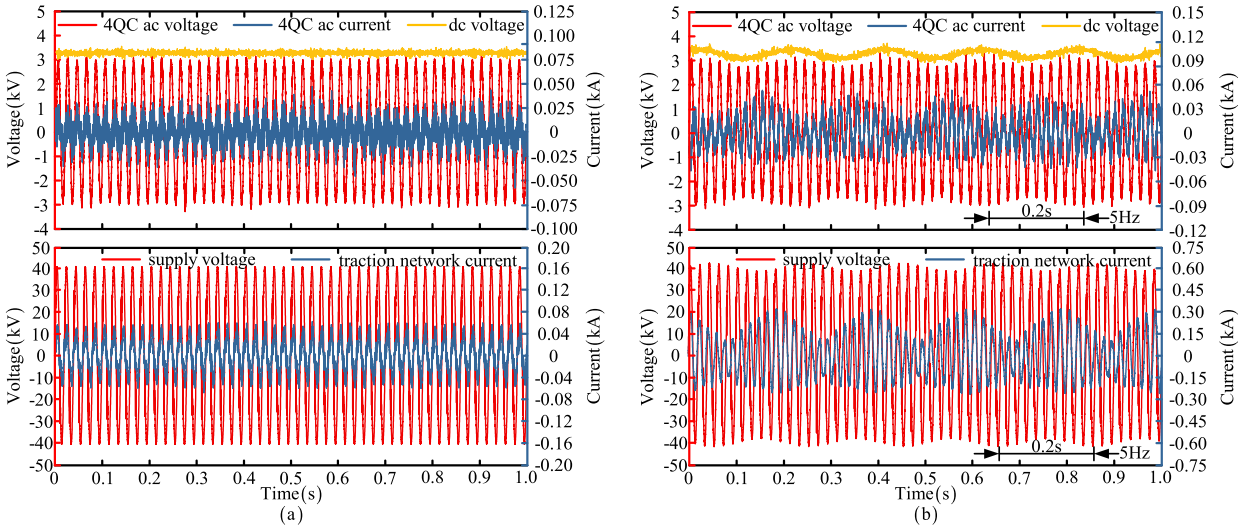

FIGURE 1. Field test measurements of the September 2010 LFO incident in the Qingdao EMU operation depot. (a) 5 CRH5 EMUs (no LFO) and (b) 6 CRH5 EMUs (LFO) were put into operation[1].

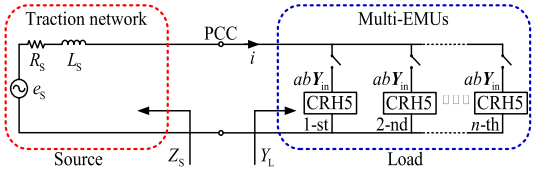

FIGURE 2. Cascaded structure of an NTS.

tance in parallel; the position between the two parts is defined as the point of common coupling (PCC) of the system.

Seen from the PCC, Z_S and Y_L are the equivalent source impedance and load admittance, respectively. On the source side, e_S is the voltage of the electrical substation (ESS), R_S and L_S form the equivalent impedance that includes both the ESS and the feeding network. On the load side, $\boldsymbol{Y}_{in}$ represents the input admittance matrix of a 4QC, a is the number of power units of an EMU train and b is the number of 4QCs of a power unit. Specifically for CRH5, a equals to 5 and b equals to 2 [4]. The current i stands for the total current of multiple EMUs drawn from traction network.

According to the Kirchhoff's voltage law, the system can be expressed as:

$$e_S - i\left(Z_S + \frac{1}{Y_L}\right) = 0 \tag{1}$$

Applying the Laplace transformation to (1), the relation between the e_S and i can be obtained:

$$\boldsymbol{G}_{i-e_S} = \frac{\boldsymbol{I}(s)}{\boldsymbol{E}_S(s)} = \frac{\boldsymbol{Y}_L(s)}{\boldsymbol{I}_{2\times 2} + \boldsymbol{Z}_S(s)\,\boldsymbol{Y}_L(s)} \tag{2}$$

where $\boldsymbol{I}_{2\times 2}$ is a second-order identity matrix.

[1]Since the measurement potential and current transformers (PTs and CTs) are available on the primary side of the on-board transformer of the EMU train, the 4QC ac voltage and ac current of Fig. 1 are converted from the primary side. Thus, the 4QC ac current is the combination of the three pairs of 4QCs connected by the same on-board transformer as shown in Fig. 5.

To form the $\boldsymbol{Y}_L$ model, the input admittance matrix $\boldsymbol{Y}_{in-PI}$ of EMU 4QC is introduced [11], in which the PI based controller is considered in the dq frame. Thus, the $\boldsymbol{Y}_L$ is modeled in dq frames as:

$$\boldsymbol{Y}_{Ldq-PI}(s) = abn\boldsymbol{Y}_{in\text{-}PI}(s) = m\boldsymbol{Y}_{in\text{-}PI}(s) = \begin{bmatrix} Y_{dd} & Y_{dq} \\ Y_{qd} & Y_{qq} \end{bmatrix}_{-PI} \tag{3}$$

where n is the number of EMUs, $m = abn$ is the total amount of 4QCs under the supply.

There are different methods to form the Z_S model, e.g. equivalent circuit model [22], chain-circuit model [23] and generalized symmetrical component model [24]. Regardless of the modeling method, a traction network can be treated as a linear system for LFO study, so that it can be represented by a simple expression [4]:

$$Z_S = R_S + j\omega L_S \tag{4}$$

Then, this network impedance can also be transferred into the dq frame:

$$\boldsymbol{Z}_{Sdq}(s) = \begin{bmatrix} Z_{dd} & Z_{dq} \\ Z_{qd} & Z_{qq} \end{bmatrix} = \begin{bmatrix} R_S + sL_S & -\omega L_S \\ \omega L_S & R_S + sL_S \end{bmatrix} \tag{5}$$

Generally, the "source-load" system can be synthetically described by a return-ratio matrix [25], [26]:

$$\boldsymbol{L}_{dq\text{-}PI}(s) = \boldsymbol{Z}_{Sdq}(s)\boldsymbol{Y}_{Ldq\text{-}PI}(s) \tag{6}$$

where $\boldsymbol{L}_{dq-PI}$ denotes the return-ratio matrix of the NTS in dq frame based on PI controller.

It is noted that in the calculations of this work, the basic network parameters of (5) are acquired from the field test of the LFO incident of Section II-A; the control parameters based on the conventional PI of (3) are derived from [4]. All these parameters are provided in Appendix A.

C. STABILITY ANALYSIS BY G-SUM NORM CRITERION

Conventionally, a number of methods, e.g. Nyquist criterion, Bode diagram, dominant pole method, singular-value criterion [27] and d-channel criterion [28], [29], can be applied to a cascaded MIMO system described by a return-ratio matrix of (6) for the purposes of stability studies. However, because of the multiplication of the matrices in (6), it is difficult to get the eigenvalues/poles of the system, which are key information of those methods.

Alternatively, norm criteria with the with the advantages of simpler calculation while being less conservative than other norm criteria, become an option. In this paper, a G-sum norm criterion is introduced to analyze the NTS, which calculates the G-norm and sum-norm for individual network model of (5) and train model of (3) avoiding the matrix multiplication of (6) [25], [26].

According to the G-sum norm criterion, a stable condition for an MIMO system is:

$$\left(\left\|\boldsymbol{Z}_{\mathrm{Sdq}}\right\|_{G}\cdot\left\|\boldsymbol{Y}_{\mathrm{Ldq}}\right\|_{sum}<1\right)\cup\left(\left\|\boldsymbol{Y}_{\mathrm{Ldq}}\right\|_{G}\cdot\left\|\boldsymbol{Z}_{\mathrm{Sdq}}\right\|_{sum}<1\right) \tag{7}$$

where subscripts G and sum denote the types of matrix norm. The G-sum norm criterion in this paper needs to be defined as follows:

(a) G norm of matrix: $\|\boldsymbol{H}\|_{\mathrm{G}}=\max_{ij}\left|h_{ij}\right|$

(b) sum norm of matrix: $\|\boldsymbol{H}\|_{\mathrm{sum}}=\sum_{i}\sum_{j}\left|h_{ij}\right|$

where $\boldsymbol{H}$ is a matrix, h_{ij} is the matrix element, i and j represent the matrix row and column respectively.

In other words, the system is stable when satisfying at least one of the two sub-criteria:

$$\left\|\boldsymbol{Z}_{\mathrm{Sdq}}\right\|_{G}\cdot\left\|\boldsymbol{Y}_{\mathrm{Ldq}}\right\|_{sum}<1 \tag{8a}$$

$$\left\|\boldsymbol{Y}_{\mathrm{Ldq}}\right\|_{G}\cdot\left\|\boldsymbol{Z}_{\mathrm{Sdq}}\right\|_{sum}<1 \tag{8b}$$

The G-sum criterion is a sufficient condition for system stability, however it provides a conservative evaluation. This means that there might be stable systems that do not satisfy the criterion. However, due to simpler calculations, the G-sum norm criterion can provide a quick evaluation of the NTS stability.

Considering the system established in the previous subsection, the left sides of (8a) and (8b) are calculated across a frequency range, obtaining two curves (red and blue, respectively) in Fig. 3. Consequently, the NTS is stable when any of the two curves is below 0 dB. For one EMU [Fig. 3(a)], the maximum points of both curves are below 0 dB (−14.89 dB, −9.16 dB), thus the NTS is stable. For 5 EMUs [Fig. 3(b)], although the maximum point of the blue curve is above 0 dB (4.82 dB), the red one remains below 0 dB (−0.91 dB), thus the system is still stable. For 6 EMUs [Fig. 3(c)], both curves are above 0 dB (0.67 dB, 6.41 dB), as a result, the system becomes unstable.

Detailed stability analysis results of the NTS with PI-based control is given Fig. 4. The maximum values of both curves monotonically increase with the number of EMUs. For this

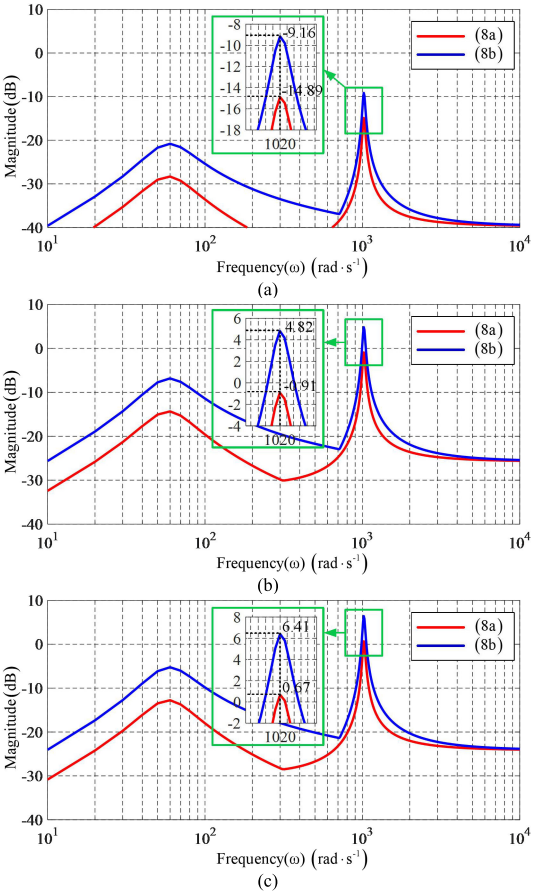

FIGURE 3. Stability analysis of the NTS with PI-based control. (a) One EMU [stable], (b) 5 EMUs [stable], (c) 6 EMUs [unstable] are put into operation.

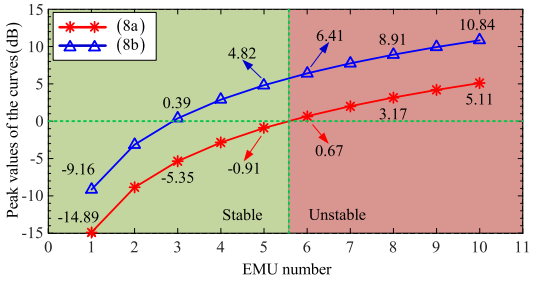

FIGURE 4. The stability analysis of the NTS with PI-based control when the EMU number changes.

supply network, the critical LFO condition is that 6 EMUs are put into operation simultaneously. The stability analysis indicates that putting more EMUs into operation under a same supply may lead to instability. In fact, (3) explains that the number of 4QCs/EMUs essentially affects the multi-EMUs admittance $\boldsymbol{Y}_{\mathrm{Ldq-PI}}$ which consists of all the 4QC admittance $\boldsymbol{Y}_{\mathrm{in-PI}}$. Furthermore, $\boldsymbol{Y}_{\mathrm{in-PI}}$ is quite related to the control parameters, as established in [11].

III. A PBC-SMS CONTROL FOR LFO SUPPRESSION

A. SYSTEM CONFIGURATION AND 4QC MODELING

An NTS of HSRs is shown in Fig. 5 where the traction network is powered by a three-phase grid through a traction

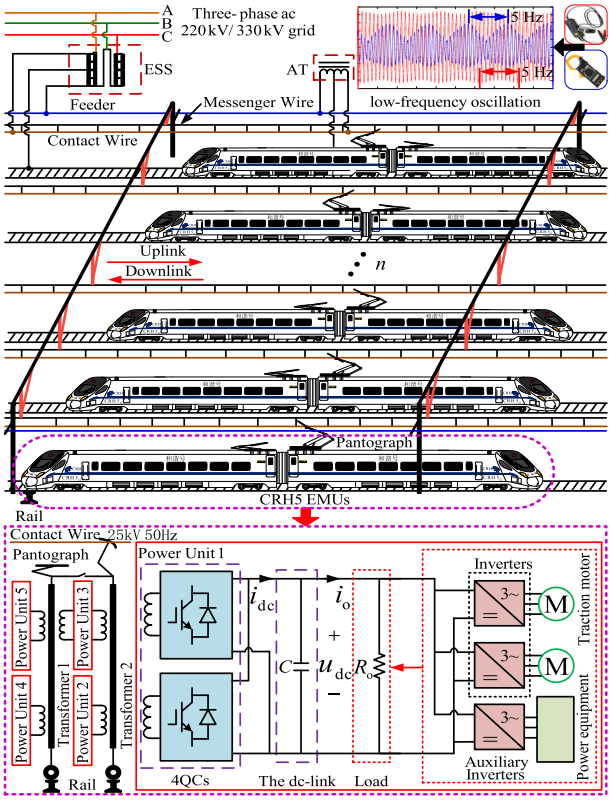

FIGURE 5. Configuration of network-train system of high-speed railways.

transformer installed in the ESS. An EMU train draws power from the overhead line through a pantograph, supplying its traction system. The traction system is divided in identical units placed in different carriages and interleaved via two multi-winding transformers on board the train.[2] In each unit, two interleaved single-phase 4QCs sharing a common dc-link play the role of network side power conversion; two three-phase inverters for motor driving and an auxiliary inverter powering the rest of EMUs are connected to the dc-link in parallel.

When discussing NTS issues, an EMU is generally modeled by its network-side power conversion, i.e. the 4QCs. Since the LFO incidents usually happen in railway stations or EMU depots when EMUs are under light or no traction load [30], [31], only 4QCs and auxiliary inverters are in operation. This can be simply modeled as a resistive load at the dc-link (R_o in Fig. 5) [32], [33]. Assuming that in an EMU every 4QCs share an average power and all have identical network side circuits, each 4QC can be modeled as shown in Fig. 6.

In Fig. 6, u_S and i_S represent the network side voltage and current, r_L and L stand for the equivalent impedance of secondary winding of the on-board transformer. u_{ab} and u_{dc} are the 4QC ac- and dc- side voltages. As there are two converters in a power unit, the dc side is model as $i_{dc}/2, i_o/2, C/2$ and $2R_o$ (Fig. 6).

[2]The power unit 3 of Fig. 4 can be powered by either of the two on-board transformers. The power unit 3 was powered by transformer 2 in this paper.

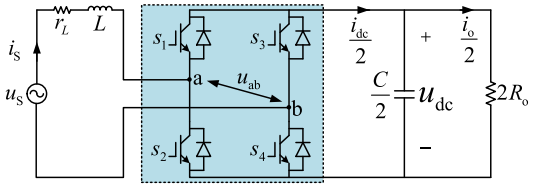

FIGURE 6. The equivalent circuit of the single-phase EMU 4QC.

The state space equations of the 4QC can be expressed as:

$$\begin{cases} L\dfrac{\mathrm{d}i_S}{\mathrm{d}t} = u_S - r_L i_S - s_{ab}u_{dc} \\ C\dfrac{\mathrm{d}u_{dc}}{2\mathrm{d}t} = s_{ab}i_S - \dfrac{i_o}{2} \end{cases} \tag{9}$$

where $s_{ab} = \{-1, 0, 1\}$ is the 4QC switching function. The 4QC model of (9) can be converted into the dq frame [34], [35] as:

$$\begin{cases} L\dfrac{\mathrm{d}i_d}{\mathrm{d}t} = u_{Sd} - r_L i_d + \omega L i_q - s_{abd}u_{dc} \\ L\dfrac{\mathrm{d}i_q}{\mathrm{d}t} = u_{Sq} - r_L i_q - \omega L i_d - s_{abq}u_{dc} \\ C\dfrac{\mathrm{d}u_{dc}}{\mathrm{d}t} = -i_o + \left(s_{abd}i_d + s_{abq}i_q\right) \end{cases} \tag{10}$$

where u_{Sd}, u_{Sq}, i_d, i_q, s_{abd} and s_{abq} are the d- and q- components of u_S, i_S and of s_{ab} (periodic average), respectively.

The Euler-Lagrange (EL) mathematical model of the 4QC can be described as:

$$\boldsymbol{u}_S = \boldsymbol{M}\dot{\boldsymbol{x}} + \boldsymbol{R}\boldsymbol{x} + \boldsymbol{J}\boldsymbol{x} \tag{11}$$

where $\boldsymbol{x}$ and $\boldsymbol{u}_S$ are defined as the state and input vectors; $\boldsymbol{M}$, $\boldsymbol{R}$ and $\boldsymbol{J}$ are coefficient matrices, given as:

$$\boldsymbol{u}_S = \begin{bmatrix} u_{Sd} \\ u_{Sq} \\ 0 \end{bmatrix}; \quad \boldsymbol{x} = \begin{bmatrix} i_d \\ i_q \\ u_{dc} \end{bmatrix}; \quad \boldsymbol{J} = \begin{bmatrix} 0 & -\omega L & s_{abd} \\ \omega L & 0 & s_{abq} \\ s_{abd} & s_{abq} & 0 \end{bmatrix}$$
$$\boldsymbol{M} = \mathrm{diag}\begin{bmatrix} L & L & -C \end{bmatrix}; \quad \boldsymbol{R} = \mathrm{diag}\begin{bmatrix} r_L & r_L & -\dfrac{1}{R_o} \end{bmatrix} \tag{12}$$

It is seen that $\boldsymbol{M}$ is a positive definite diagonal matrix, which represents the energy storage elements of the system; $\boldsymbol{R}$ is a positive definite diagonal matrix, which represents the dissipation characteristics of a 4QC; $\boldsymbol{J}$ is an anti-symmetric matrix, representing the interaction among the state variables. Based on the system modeled above, a PBC-SMS control strategy is then proposed for LFO suppression.

B. CONTROL LAW OF DC VOLTAGE BASED ON SMS

The SMS is especially suitable for the closed-loop control of power conversion systems. Controllers based on SMS are easy to design and implement, and they possess good robustness and dynamic performance [35]. For better dynamic performance, the 4QC dc voltage can be controlled under

the SMS. For ensuring unity power factor and constant dc voltage [20], [36], the sliding mode £ is defined as:

$$£=\begin{cases} £_i\left(\varepsilon_{i_q},t\right)=k_3\left(i_q^*-i_q\right)=0 \\ £_u\left(\varepsilon_{u_{dc}},\varepsilon_{u'_{dc}},t\right)=k_1\left(u_{dc}^*-u_{dc}\right)+k_2\left(u_{dc}'^*-u'_{dc}\right)=0 \end{cases} \tag{13}$$

where $£_i$ and $£_u$ are the current and voltage components of £, u'_{dc} is the first-order derivative of u_{dc}; $\varepsilon_{u_{dc}}=u_{dc}^*-u_{dc}$, $\varepsilon_{i_q}=i_q^*-i_q$, $\varepsilon_{u'_{dc}}=u_{dc}'^*-u'_{dc}$ are the deviation variables corresponding to u_{dc}, i_q and u'_{dc}; k_1, k_2 and k_3 are the controller gains. Considering some non-modeled dynamics (e.g. dead-time, semiconductor delays), the value of k_2/k_1 cannot be set too large [36].

Substituting (10) into (13):

$$i_d=\frac{C}{k_2 s_{abd}}\left[k_1\left(u_{dc}^*-u_{dc}\right)+\frac{k_2}{C}\left(\frac{u_{dc}}{R_o}-s_{abq}i_q\right)\right] \tag{14}$$

When a 4QC reaches an equilibrium point, di_d/dt, di_q/dt, i_q and u_{Sq} are equal to zero. Thus, from (10) the switching function of 4QC can be obtained:

$$s_{abq}=-\frac{\omega L i_d}{u_{dc}},\quad s_{abd}=\frac{u_{Sd}-R_o i_d}{u_{dc}} \tag{15}$$

Substituting (15) into (14), it follows that:

$$i_d=\frac{Cu_{dc}}{k_2\left(u_{Sd}-r_L i_d\right)}\left[k_1\left(u_{dc}^*-u_{dc}\right)+\frac{k_2 i_o}{C}\right] \tag{16}$$

When the sliding mode £ tends to zero, i_d will equal to i_d^*. Therefore, the control law of the outer voltage loop under SMS is:

$$i_d^*=\frac{Cu_{dc}}{k_2\left(u_{Sd}-r_L i_d^*\right)}\left[k_1\left(u_{dc}^*-u_{dc}\right)+\frac{k_2 i_o}{C}\right] \tag{17}$$

In (17), k_1 and k_2 are the controller gains. Taking into account the dead-time and semiconductor delays of the switches, their values should not be too large [36].

C. CONTROL LAW OF AC CURRENT BASED ON PBC

The PBC has the advantages of high stability globally in a nonlinear system, strong robustness to the system parameters deviation, and it possesses good steady-state performance. The 4QC ac current is controlled by PBC, realizing zero steady-state tracking. An energy storage function of a 4QC can be defined as:

$$\boldsymbol{H}(\boldsymbol{x})=\frac{1}{2}\boldsymbol{x}^T\boldsymbol{M}\boldsymbol{x} \tag{18}$$

Substituting (11) into the first-order derivative of (18), an expression reflecting the energy dissipation rate is obtained:

$$\dot{\boldsymbol{H}}(\boldsymbol{x})=\boldsymbol{x}^{\mathrm{T}}\boldsymbol{M}\dot{\boldsymbol{x}}=\boldsymbol{x}^{\mathrm{T}}\left(\boldsymbol{u}_{\mathrm{S}}-\boldsymbol{R}\boldsymbol{x}-\boldsymbol{J}\boldsymbol{x}\right)=\boldsymbol{u}_{\mathrm{S}}^{\mathrm{T}}\boldsymbol{x}-\boldsymbol{x}^{\mathrm{T}}\boldsymbol{R}\boldsymbol{x} \tag{19}$$

Selecting the state as the output, i.e. $\boldsymbol{y}=\boldsymbol{x}$, a dissipative inequality is satisfied [37]:

$$\dot{\boldsymbol{H}}(\boldsymbol{x})\le\boldsymbol{u}_{\mathrm{S}}^{\mathrm{T}}\boldsymbol{y}-\boldsymbol{x}^{\mathrm{T}}\boldsymbol{R}\boldsymbol{x} \tag{20}$$

where $\dot{\boldsymbol{H}}(\boldsymbol{x})$ represents the energy storage rate, $\boldsymbol{u}_{\mathrm{S}}^{\mathrm{T}}\boldsymbol{y}$ represents the energy supply rate to the 4QCs, $\boldsymbol{x}^{\mathrm{T}}\boldsymbol{R}\boldsymbol{x}$ represents the energy dissipation rate in the 4QCs. Therefore, the 4QC is strictly passive.

Similarly, a storage function for the state error $\boldsymbol{x}_{\mathrm{e}}=\boldsymbol{x}-\boldsymbol{x}^*$ is defined as:

$$\boldsymbol{H}_{\mathrm{e}}(\boldsymbol{x}_{\mathrm{e}})=\frac{1}{2}\boldsymbol{x}_{\mathrm{e}}^{\mathrm{T}}\boldsymbol{M}\boldsymbol{x}_{\mathrm{e}} \tag{21}$$

Then, (11) can be converted to:

$$\boldsymbol{M}\dot{\boldsymbol{x}}_{\mathrm{e}}+\boldsymbol{R}\boldsymbol{x}_{\mathrm{e}}+\boldsymbol{J}\boldsymbol{x}_{\mathrm{e}}=\boldsymbol{u}_{\mathrm{S}}-\left(\boldsymbol{M}\dot{\boldsymbol{x}}^*+\boldsymbol{R}\boldsymbol{x}^*+\boldsymbol{J}\boldsymbol{x}^*\right) \tag{22}$$

For ensuring state tracking, the energy dissipation should be sped up. Consequently, additional damping can be injected into the system for fast error convergence towards zero, i.e. $\boldsymbol{H}_{\mathrm{e}}(\boldsymbol{x}_{\mathrm{e}})\to 0$. Thus, a total damping matrix is defined as:

$$\boldsymbol{R}_{\mathrm{I}}=\boldsymbol{R}+\boldsymbol{R}_{\mathrm{a}} \tag{23}$$

where $\boldsymbol{R}_{\mathrm{a}}=\mathrm{diag}\begin{bmatrix} r_1 & r_2 & r_3 \end{bmatrix}$ is the injected damping.

With the damping injection, (22) becomes to:

$$\boldsymbol{M}\dot{\boldsymbol{x}}_{\mathrm{e}}+\boldsymbol{R}_{\mathrm{I}}\boldsymbol{x}_{\mathrm{e}}+\boldsymbol{J}\boldsymbol{x}_{\mathrm{e}}=\boldsymbol{u}_{\mathrm{S}}-\left(\boldsymbol{M}\dot{\boldsymbol{x}}^*+\boldsymbol{R}\boldsymbol{x}^*+\boldsymbol{J}\boldsymbol{x}^*-\boldsymbol{R}_{\mathrm{a}}\boldsymbol{x}_{\mathrm{e}}\right) \tag{24}$$

Therefore, the inner current loop PBC law of the 4QC can be derived as:

$$\boldsymbol{u}_{\mathrm{S}}=\boldsymbol{M}\dot{\boldsymbol{x}}^*+\boldsymbol{R}\boldsymbol{x}^*+\boldsymbol{J}\boldsymbol{x}-\boldsymbol{R}_{\mathrm{a}}\boldsymbol{x}_{\mathrm{e}} \tag{25}$$

Substituting (25) into (24), it follows that:

$$\boldsymbol{M}\dot{\boldsymbol{x}}_{\mathrm{e}}+\boldsymbol{R}_{\mathrm{I}}\boldsymbol{x}_{\mathrm{e}}=0 \tag{26}$$

Therefore, the storage rate for state error of the system satisfies:

$$\dot{\boldsymbol{H}}_{\mathrm{e}}(\boldsymbol{x}_{\mathrm{e}})=\boldsymbol{x}_{\mathrm{e}}^{\mathrm{T}}\boldsymbol{M}\dot{\boldsymbol{x}}_{\mathrm{e}}=-\boldsymbol{x}_{\mathrm{e}}^{\mathrm{T}}\boldsymbol{R}_{\mathrm{I}}\boldsymbol{x}_{\mathrm{e}}=-\boldsymbol{x}_{\mathrm{e}}^{\mathrm{T}}\left(\boldsymbol{R}+\boldsymbol{R}_{\mathrm{a}}\right)\boldsymbol{x}_{\mathrm{e}}<0 \tag{27}$$

Since $\boldsymbol{R}_{\mathrm{I}}$ is a positive definite diagonal matrix, the storage for state error of the system $\boldsymbol{H}_{\mathrm{e}}(\boldsymbol{x}_{\mathrm{e}})$ must converge to zero.

According to (12) and (25), the inner current loop PBC law of the EMU 4QC can be finally decided:

$$\begin{cases} u_d=u_{Sd}+r_1 i_d-\left(r_L+r_1\right)i_d^*+\omega L i_q \\ u_q=u_{Sq}+r_2 i_q-\left(r_L+r_2\right)i_q^*-\omega L i_d \end{cases} \tag{28}$$

In (28), there is a trade-off in tuning the r_1 and r_2. The larger their values, the faster the system converges, i.e. a good dynamic response. However, too large values may lead to over-modulation and higher harmonics [36]. On the other hand, smaller r_1 and r_2 values can improve steady-state performance.

According to the outer voltage loop SMS control law of (17) and the inner current loop PBC law of (28), a PBC-SMS control strategy for 4QC is proposed. Fig. 7 presents the entire structure of the PBC-SMS strategy where the phase-lock loop (PLL) and imaginary orthogonal generation are based on the second-order generalized integrator (SOGI) [4], and a conventional carrier based PWM scheme (with 250 Hz carrier frequency of CRH5 model) is adopted. It is seen that there are only four parameters in the proposed control system; equal to conventional PI-based control [11], and fewer than the ADRC [13] or ESO+MPC [16]. Generally, k_1 and k_2 are set equal to each other [36], and from (28) the values

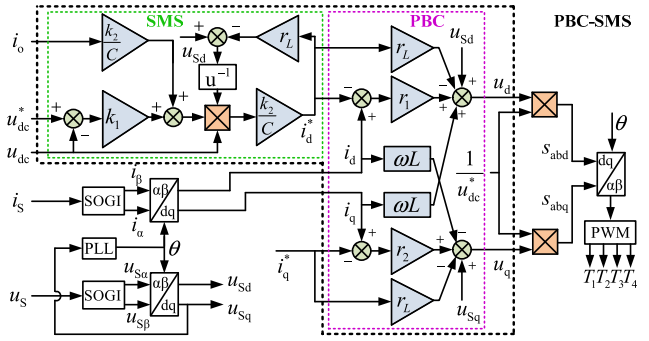

FIGURE 7. The proposed PBC-SMS control strategy for EMU 4QC.

r_1 and r_2 can be seen identical, i.e. only two of these values need to be considered. Taking into account both the dynamic and steady-state performance, reiterative simulation tuning process is generally needed for getting appropriate these two parameters, and their values, used in stability and simulation of this work, are givenx in Appendix A.

IV. STABILITY ANALYSIS FOR PBC-SMS

A. 4QC MODELING WITH PBC-SMS

In order to analyze the NTS stability with proposed PBC-SMS, the small-signal method is employed for modeling the EMU 4QC.

The steady-state form of (10) is:

$$\begin{cases} 0 = U_{\mathrm{Sd}} - r_L I_{\mathrm{d}} + \omega L I_{\mathrm{q}} - S_{\mathrm{abd}} U_{\mathrm{dc}} \\ 0 = U_{\mathrm{Sq}} - r_L I_{\mathrm{q}} - \omega L I_{\mathrm{d}} - S_{\mathrm{abq}} U_{\mathrm{dc}} \\ 0 = -U_{\mathrm{dc}}/R_{\mathrm{o}} + S_{\mathrm{abd}} I_{\mathrm{d}} + S_{\mathrm{abq}} I_{\mathrm{q}} \end{cases} \tag{29}$$

where U_{Sd} equals to the amplitude of u_{S}, u_{Sq} equals to zero, so does the U_{Sq}. The EMU 4QC is required to work under unity power factor, so I_{q} equals to zero as well. Then, given the values of U_{Sd} and U_{dc}, the steady-state values of I_{d}, S_{abd} and S_{abq} can be obtained from (29), as shown in (30):

$$\begin{aligned} S_{\mathrm{abd}} &= \frac{U_{\mathrm{Sd}} + \sigma}{2U_{\mathrm{dc}}}, \quad S_{\mathrm{abq}} = -\frac{\omega L (U_{\mathrm{Sd}} - \sigma)}{2 r_L U_{\mathrm{dc}}}, \\ I_{\mathrm{d}} &= \frac{U_{\mathrm{Sd}} - \sigma}{2 r_L} \end{aligned} \tag{30}$$

where $\sigma = \sqrt{U_{\mathrm{Sd}}^2 - \frac{4 r_L}{R_{\mathrm{o}}} U_{\mathrm{dc}}^2}$.

Each variable in (10) is regarded as a steady-state variable plus a small-signal variable, (10) can be rewritten as:

$$\begin{cases} L \dfrac{\mathrm{d}\left(I_{\mathrm{d}} + \hat{i}_{\mathrm{d}}\right)}{\mathrm{d}t} = \left(U_{\mathrm{Sd}} + \hat{u}_{\mathrm{Sd}}\right) - r_L \left(I_{\mathrm{d}} + \hat{i}_{\mathrm{d}}\right) + \omega L \left(I_{\mathrm{q}} + \hat{i}_{\mathrm{q}}\right) \\ \qquad - \left(S_{\mathrm{abd}} + \hat{s}_{\mathrm{abd}}\right)\left(U_{\mathrm{dc}} + \hat{u}_{\mathrm{dc}}\right) \\ L \dfrac{\mathrm{d}\left(I_{\mathrm{q}} + \hat{i}_{\mathrm{q}}\right)}{\mathrm{d}t} = \left(U_{\mathrm{Sq}} + \hat{u}_{\mathrm{Sq}}\right) - r_L \left(I_{\mathrm{q}} + \hat{i}_{\mathrm{q}}\right) - \omega L \left(I_{\mathrm{d}} + \hat{i}_{\mathrm{d}}\right) \\ \qquad - \left(S_{\mathrm{abq}} + \hat{s}_{\mathrm{abq}}\right)\left(U_{\mathrm{dc}} + \hat{u}_{\mathrm{dc}}\right) \\ C \dfrac{\mathrm{d}\left(U_{\mathrm{dc}} + \hat{u}_{\mathrm{dc}}\right)}{\mathrm{d}t} = -\dfrac{\left(U_{\mathrm{dc}} + \hat{u}_{\mathrm{dc}}\right)}{R_{\mathrm{o}}} + \left(S_{\mathrm{abd}} + \hat{s}_{\mathrm{abd}}\right)\left(I_{\mathrm{d}} + \hat{i}_{\mathrm{d}}\right) \\ \qquad + \left(S_{\mathrm{abq}} + \hat{s}_{\mathrm{abq}}\right)\left(I_{\mathrm{q}} + \hat{i}_{\mathrm{q}}\right) \end{cases} \tag{31}$$

where the variables with hat denote the corresponding small-signal values.

Substituting (29) into (31), and ignoring the product term of the small-signal variables, the small-signal model of the single EMU 4QC can be obtained as:

$$\begin{aligned} \frac{\mathrm{d}}{\mathrm{d}t}\begin{bmatrix} \hat{i}_{\mathrm{d}} \\ \hat{i}_{\mathrm{q}} \\ \hat{u}_{\mathrm{dc}} \end{bmatrix} &= \begin{bmatrix} -\dfrac{r_L}{L} & \omega & -\dfrac{S_{\mathrm{abd}}}{L} \\ -\omega & -\dfrac{r_L}{L} & -\dfrac{S_{\mathrm{abq}}}{L} \\ \dfrac{S_{\mathrm{abd}}}{C} & \dfrac{S_{\mathrm{abq}}}{C} & -\dfrac{1}{CR_{\mathrm{o}}} \end{bmatrix} \begin{bmatrix} \hat{i}_{\mathrm{d}} \\ \hat{i}_{\mathrm{q}} \\ \hat{u}_{\mathrm{dc}} \end{bmatrix} \\ &+ \begin{bmatrix} -\dfrac{U_{\mathrm{dc}}}{L} & 0 \\ 0 & -\dfrac{U_{\mathrm{dc}}}{L} \\ \dfrac{I_{\mathrm{d}}}{C} & \dfrac{I_{\mathrm{q}}}{C} \end{bmatrix} \begin{bmatrix} \hat{s}_{\mathrm{abd}} \\ \hat{s}_{\mathrm{abq}} \end{bmatrix} \\ &+ \begin{bmatrix} \dfrac{1}{L} & 0 \\ 0 & \dfrac{1}{L} \\ 0 & 0 \end{bmatrix} \begin{bmatrix} \hat{u}_{\mathrm{Sd}} \\ \hat{u}_{\mathrm{Sq}} \end{bmatrix} \end{aligned} \tag{32}$$

The matrix form of (32) is:

$$\dot{\hat{\boldsymbol{x}}} = \boldsymbol{A}\hat{\boldsymbol{x}} + \boldsymbol{B}\hat{\boldsymbol{s}} + \boldsymbol{C}\hat{\boldsymbol{u}}_{\mathrm{S}} \tag{33}$$

in which, $\boldsymbol{A}, \boldsymbol{B}$ and $\boldsymbol{C}$ are the corresponding coefficient matrices of the small-signal variables $\hat{\boldsymbol{x}} = [\hat{i}_{\mathrm{d}}, \hat{i}_{\mathrm{q}}, \hat{u}_{\mathrm{dc}}]^{\mathrm{T}}$, $\hat{\boldsymbol{s}} = [\hat{s}_{\mathrm{abd}}, \hat{s}_{\mathrm{abq}}]^{\mathrm{T}}$ and $\hat{\boldsymbol{u}}_{\mathrm{S}} = [\hat{u}_{\mathrm{Sd}}, \hat{u}_{\mathrm{Sq}}]^{\mathrm{T}}$, respectively.

Eq. (33) can be transformed into the frequency domain by Laplace transform:

$$\hat{\boldsymbol{x}} = (s\boldsymbol{I}_{3\times 3} - \boldsymbol{A})^{-1}\boldsymbol{B}\hat{\boldsymbol{s}} + (s\boldsymbol{I}_{3\times 3} - \boldsymbol{A})^{-1}\boldsymbol{C}\hat{\boldsymbol{u}}_{\mathrm{S}} \tag{34}$$

where $\boldsymbol{I}_{3\times 3}$ is a third-order identity matrix.

In steady-state, the output of the SMS voltage loop is d-axis current reference i_{d}^*, which satisfies:

$$I_{\mathrm{d}}^* = \frac{C U_{\mathrm{dc}}}{k_2 \left(U_{\mathrm{Sd}} - r_L I_{\mathrm{d}}\right)} \left[k_1 \left(U_{\mathrm{dc}}^* - U_{\mathrm{dc}}\right) + \frac{k_2 U_{\mathrm{dc}}}{C R_{\mathrm{o}}} \right] \tag{35}$$

The state variables in (17) are expressed as steady-state variables plus small-signal variables, so that:

$$\begin{aligned} & I_{\mathrm{d}}^* + \hat{i}_{\mathrm{d}}^* \\ &= \frac{C\left(U_{\mathrm{dc}} + \hat{u}_{\mathrm{dc}}\right)}{k_2 \left[\left(U_{\mathrm{Sd}} + \hat{u}_{\mathrm{Sd}}\right) - r_L \left(I_{\mathrm{d}} + \hat{i}_{\mathrm{d}}\right)\right]} \\ &\quad \times \left\{ k_1 \left[\left(U_{\mathrm{dc}}^* + \hat{u}_{\mathrm{dc}}^*\right) - \left(U_{\mathrm{dc}} + \hat{u}_{\mathrm{dc}}\right)\right] + \frac{k_2 \left(U_{\mathrm{dc}} + \hat{u}_{\mathrm{dc}}\right)}{C R_{\mathrm{o}}} \right\} \end{aligned} \tag{36}$$

Substituting (35) into (36), and again ignoring the product term of the small-signal variables, the small-signal model of the outer voltage loop SMS control law can be obtained as:

$$\hat{i}_{\mathrm{d}}^* = \frac{\left(\frac{2k_2}{R_{\mathrm{o}}} - k_1 C\right) U_{\mathrm{dc}} \hat{u}_{\mathrm{dc}} - k_2 I_{\mathrm{d}}^* \hat{u}_{\mathrm{Sd}} + k_2 r_L I_{\mathrm{d}}^* \hat{i}_{\mathrm{d}}}{k_2 U_{\mathrm{Sd}} - k_2 r_L I_{\mathrm{d}}} \tag{37}$$

In steady-state, the inner current loop PBC law (28) satisfies:

$$\begin{cases} U_{\mathrm{d}} = U_{\mathrm{Sd}} + r_1 I_{\mathrm{d}} - (r_L + r_1)\, I_{\mathrm{d}}^* + \omega L I_{\mathrm{q}} \\ U_{\mathrm{q}} = U_{\mathrm{Sq}} + r_2 I_{\mathrm{q}} - (r_L + r_2)\, I_{\mathrm{q}}^* - \omega L I_{\mathrm{d}} \end{cases} \tag{38}$$

Each variable in (28) is regarded as steady-state variable plus a small-signal variable. Then, (28) can be rewritten as:

$$\begin{cases} U_{\mathrm{d}} + \hat{u}_{\mathrm{d}} = \left(U_{\mathrm{Sd}} + \hat{u}_{\mathrm{Sd}}\right) + r_1 \left(I_{\mathrm{d}} + \hat{i}_{\mathrm{d}}\right) - (r_L + r_1)\left(I_{\mathrm{d}}^* + \hat{i}_{\mathrm{d}}^*\right) \\ \qquad\qquad + \omega L \left(I_{\mathrm{q}} + \hat{i}_{\mathrm{q}}\right) \\ U_{\mathrm{q}} + \hat{u}_{\mathrm{q}} = \left(U_{\mathrm{Sq}} + \hat{u}_{\mathrm{Sq}}\right) + r_2 \left(I_{\mathrm{q}} + \hat{i}_{\mathrm{q}}\right) - (r_L + r_2)\left(I_{\mathrm{q}}^* + \hat{i}_{\mathrm{q}}^*\right) \\ \qquad\qquad - \omega L \left(I_{\mathrm{d}} + \hat{i}_{\mathrm{d}}\right) \end{cases} \tag{39}$$

Combining (37), (38) and (39), neglecting the product term of small-signal variables, the small-signal model of the inner current loop PBC law can be derived as:

$$\begin{cases} \hat{u}_{\mathrm{d}} = \hat{u}_{\mathrm{Sd}} + r_1 \hat{i}_{\mathrm{d}} - (r_L + r_1)\, \hat{i}_{\mathrm{d}}^* + \omega L \hat{i}_{\mathrm{q}} \\ \qquad = \left(r_1 - \dfrac{(r_L + r_1)\, r_L I_{\mathrm{d}}^*}{U_{\mathrm{Sd}} - r_L I_{\mathrm{d}}}\right) \hat{i}_{\mathrm{d}} \\ + \omega L \hat{i}_{\mathrm{q}} - \dfrac{(r_L + r_1)\,(2k_2 - k_1 C R_{\mathrm{o}})\, U_{\mathrm{dc}}}{(k_2 U_{\mathrm{Sd}} - k_2 r_L I_{\mathrm{d}})\, R_{\mathrm{o}}} \hat{u}_{\mathrm{dc}} \\ \qquad + \left(1 + \dfrac{(r_L + r_1)\, I_{\mathrm{d}}^*}{U_{\mathrm{Sd}} - r_L I_{\mathrm{d}}}\right) \hat{u}_{\mathrm{Sd}} \\ \hat{u}_{\mathrm{q}} = -\omega L \hat{i}_{\mathrm{d}} + r_2 \hat{i}_{\mathrm{q}} + \hat{u}_{\mathrm{Sq}} \end{cases} \tag{40}$$

According to Fig. 7, standardizing the PWM carrier by u_{dc}^*, the relationship between the switching signal $[s_{\mathrm{abd}}, s_{\mathrm{abq}}]^{\mathrm{T}}$ and $[u_{\mathrm{d}}, u_{\mathrm{q}}]^{\mathrm{T}}$ can be expressed as [11]:

$$\begin{bmatrix} s_{\mathrm{abd}} & s_{\mathrm{abq}} \end{bmatrix}^T = \frac{1}{2} \begin{bmatrix} u_{\mathrm{d}} & u_{\mathrm{q}} \end{bmatrix}^T \tag{41}$$

As a result, the small-signal model of the 4QC switching signals can be derived as:

$$\begin{aligned} \begin{bmatrix} \hat{s}_{\mathrm{abd}} \\ \hat{s}_{\mathrm{abq}} \end{bmatrix} &= \begin{bmatrix} \dfrac{r_1 - \frac{(r_L + r_1) r_L I_{\mathrm{d}}^*}{U_{\mathrm{Sd}} - r_L I_{\mathrm{d}}}}{2U_{\mathrm{dc}}^*} & \dfrac{\omega L}{2U_{\mathrm{dc}}^*} & \dfrac{-(r_L + r_1)(2k_2 - k_1 C R_{\mathrm{o}}) U_{\mathrm{dc}}}{2U_{\mathrm{dc}}^* (k_2 U_{\mathrm{Sd}} - k_2 r_L I_{\mathrm{d}}) R_{\mathrm{o}}} \\ \dfrac{-\omega L}{2U_{\mathrm{dc}}^*} & \dfrac{r_2}{2U_{\mathrm{dc}}^*} & 0 \end{bmatrix} \\ &\times \begin{bmatrix} \hat{i}_{\mathrm{d}} \\ \hat{i}_{\mathrm{q}} \\ \hat{u}_{\mathrm{dc}} \end{bmatrix} + \begin{bmatrix} \dfrac{1 + \frac{(r_L + r_1) I_{\mathrm{d}}^*}{U_{\mathrm{Sd}} - r_L I_{\mathrm{d}}}}{2U_{\mathrm{dc}}^*} & 0 \\ 0 & \dfrac{1}{2U_{\mathrm{dc}}^*} \end{bmatrix} \begin{bmatrix} \hat{u}_{\mathrm{Sd}} \\ \hat{u}_{\mathrm{Sq}} \end{bmatrix} \end{aligned} \tag{42}$$

The matrix form of (42) is:

$$\hat{\boldsymbol{s}} = \boldsymbol{D}\hat{\boldsymbol{x}} + \boldsymbol{E}\hat{\boldsymbol{u}}_{\mathrm{S}} \tag{43}$$

where $\boldsymbol{D}$ and $\boldsymbol{E}$ are defined as the coefficient matrix of the small-signal variables $\hat{\boldsymbol{x}}$ and $\hat{\boldsymbol{u}}_{\mathrm{S}}$, respectively.

Substituting (43) into (34), it follows that:

$$\begin{aligned} \begin{bmatrix} \hat{i}_{\mathrm{d}} \\ \hat{i}_{\mathrm{q}} \\ \hat{u}_{\mathrm{dc}} \end{bmatrix} &= \left[\boldsymbol{I}_{3\times 3} - (s\boldsymbol{I}_{3\times 3} - \boldsymbol{A})^{-1} \boldsymbol{B}\boldsymbol{D}\right]^{-1} (s\boldsymbol{I}_{3\times 3} - \boldsymbol{A})^{-1} \\ &\quad \times (\boldsymbol{B}\boldsymbol{E} + \boldsymbol{C}) \begin{bmatrix} \hat{u}_{\mathrm{Sd}} \\ \hat{u}_{\mathrm{Sq}} \end{bmatrix} \\ &= \begin{bmatrix} \boldsymbol{G}_{i-u_{\mathrm{S}}} \\ \boldsymbol{G}_{u_{\mathrm{dc}}-u_{\mathrm{S}}} \end{bmatrix} \begin{bmatrix} \hat{u}_{\mathrm{Sd}} \\ \hat{u}_{\mathrm{Sq}} \end{bmatrix} \end{aligned} \tag{44}$$

where $\boldsymbol{G}_{i-u_{\mathrm{S}}}$ is the 2×2 order transfer matrix from $[\hat{u}_{\mathrm{Sd}}, \hat{u}_{\mathrm{Sq}}]^{\mathrm{T}}$ to $[\hat{i}_{\mathrm{d}}, \hat{i}_{\mathrm{q}}]^{\mathrm{T}}$, and $\boldsymbol{G}_{u_{\mathrm{dc}}-u_{\mathrm{S}}}$ is a 1×2 order transfer matrix from $[\hat{u}_{\mathrm{Sd}}, \hat{u}_{\mathrm{Sq}}]^{\mathrm{T}}$ to $\hat{u}_{\mathrm{dc}}$.

The matrix form of (44) is:

$$\hat{\boldsymbol{x}} = \begin{bmatrix} \boldsymbol{G}_{i-u_{\mathrm{S}}} \\ \boldsymbol{G}_{u_{\mathrm{dc}}-u_{\mathrm{S}}} \end{bmatrix} \hat{\boldsymbol{u}}_{\mathrm{S}} \tag{45}$$

Thus, the input admittance matrix of the 4QC with PBC-SMS can be depicted as:

$$\boldsymbol{Y}_{\text{in-PBC-SMS}} = \frac{\hat{\boldsymbol{x}}_i}{\hat{\boldsymbol{u}}_{\mathrm{S}}} = \boldsymbol{G}_{i-u_{\mathrm{S}}} \tag{46}$$

where $\hat{\boldsymbol{x}}_i$ represents the current components in $\hat{\boldsymbol{x}}$.

As a result, the input admittance matrix $\boldsymbol{Y}_{\mathrm{Ldq-PBC-SMS}}$ of the multi-EMUs based on the proposed PBC-SMS is obtained as:

$$\boldsymbol{Y}_{\text{Ldq-PBC-SMS}} = abn\boldsymbol{Y}_{\text{in-PBC-SMS}} = m\boldsymbol{Y}_{\text{in-PBC-SMS}} = m\boldsymbol{G}_{i-u_{\mathrm{S}}} \tag{47}$$

B. STABILITY ANALYSIS

Using the "load" model of (47) and the "source" model of (5), the G-sum norm criterion of Section II-C is utilized once again to investigate the stability of the NTS with PBC-SMS. In this case, as shown in Fig. 8(a) where both curves are below 0 dB, the system is stable when 6 EMUs operating under the supply. With the number of EMUs increasing to 29, as shown in Fig. 8(b) where the peaks of red and blue curves are −0.19 dB and 4.49 dB, the system still keeps stable. Adding one more EMU train (for a total of 30 EMUs), as shown in Fig. 8(c), the peaks increase to 0.11 dB and 4.79 dB and, the system becomes unstable.

Similarly, detailed stability analysis results for proposed controller are illustrated in Fig. 9. It is found that 30 EMUs operating under the supply is the critical condition for this case. Comparing to the case of PI-based control investigated in Section II, the proposed PBC-SMS provides much wider stability margin for LFO suppression.

In essence, according to the stability comparison between the proposed PBC-SMS and conventional PI, it is found that the proposed control essentially reduces the EMU input admittance so as to improve the NTS stability.

V. VERIFICATION

In order to validate the proposed control, simulation results are carried out and compared to more conventional

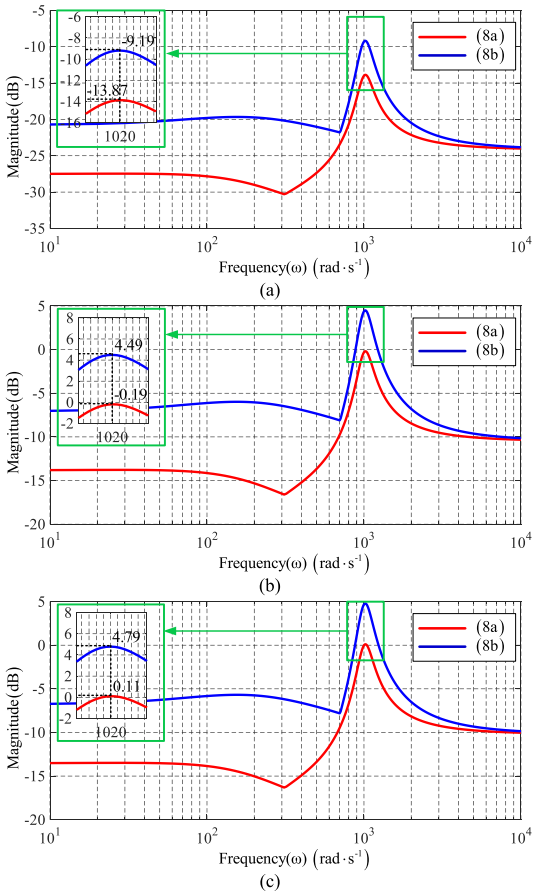

FIGURE 8. Stability analysis of the NTS with proposed PBC-SMS control. (a) 6 EMUs [stable], (b) 29 EMUs [stable], (c) 30 EMUs [unstable] are put into operation.

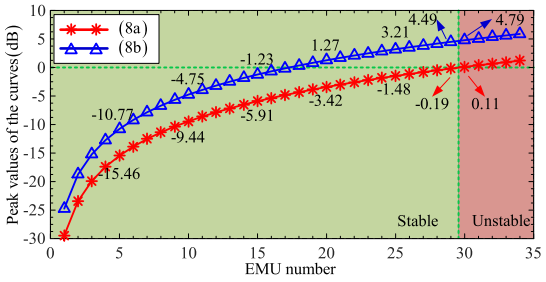

FIGURE 9. The stability analysis of the NTS with proposed PBC-SMS control when the EMU number changes.

TABLE 2. Performance indexes of the EMU 4QC dc voltage.

Methods	Overshoot (%)	Settling time (s)	Ripple (V)
PI	13.64	0.20	15
PBC	None	0.11	8
SMS	None	0.08	25
PBC-SMS	None	0.07	6

control methods. The electrical parameters used in the simulations are given in Appendix A.

A. CONTROL PERFORMANCE OF A SINGLE EMU

Firstly, the proposed PBC-SMS is tested in a single EMU train model and compared with three different methods, i.e.

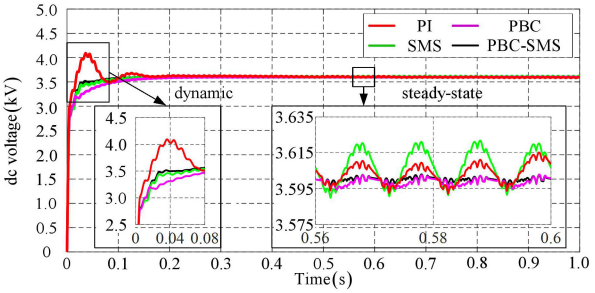

FIGURE 10. Waveforms of the single EMU 4QC dc voltage with four control strategies.

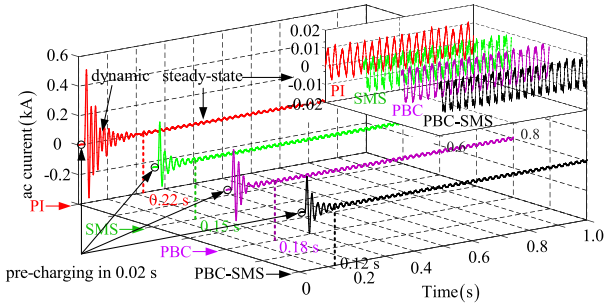

FIGURE 11. Waveforms of the single EMU ac current with four control strategies.

i) conventional PI-based control [4], ii) PBC for ac current control [18], [19] and iii) SMS for dc voltage control [20].

The EMU 4QC dc voltage waveforms of the four control methods are given in Fig. 10. In steady-state, method iii presents a large dc voltage ripple (25 V peak to peak) which is even larger than the PI case (15 V); using only PBC the ripple is reduced to 8 V; combining the two methods, the proposed PBC-SMS gives smallest ripple of 6 V. During the transient, although the PI method has a fast settle time of 0.2 s, it presents an overshoot greater than 13 %. Results of the other three methods do not show any overshoot; methods ii, iii and the proposed one reduce the settle time to 0.11 s, 0.08 s and 0.07 s, respectively. Quantitative results of the four methods are summarized in TABLE 2.

As shown in Fig. 11, since the EMU line current amplitude is very small under light or no load (about 10 A), the steady-state waveforms of the four controllers are similar; however, the settling time for start-up are different, i.e. the proposed PBC-SMS presents the shortest settling time of 0.12 s. To sum up, the proposed PBC-SMS for EMU 4QC provides smallest steady-state ripple and fastest dynamic response without overshoot.

B. LFO SUPPRESSION PERFORMANCE

To verify the LFO suppression capability of the proposed method, a second set of tests for multi-EMUs operating under a common supply network are carried out.

1) CONVENTIONAL PI CONTROLLER

For the case of conventional PI-based control used for EMU 4QCs, the results are given in Fig. 12. As shown in Fig. 12(a),

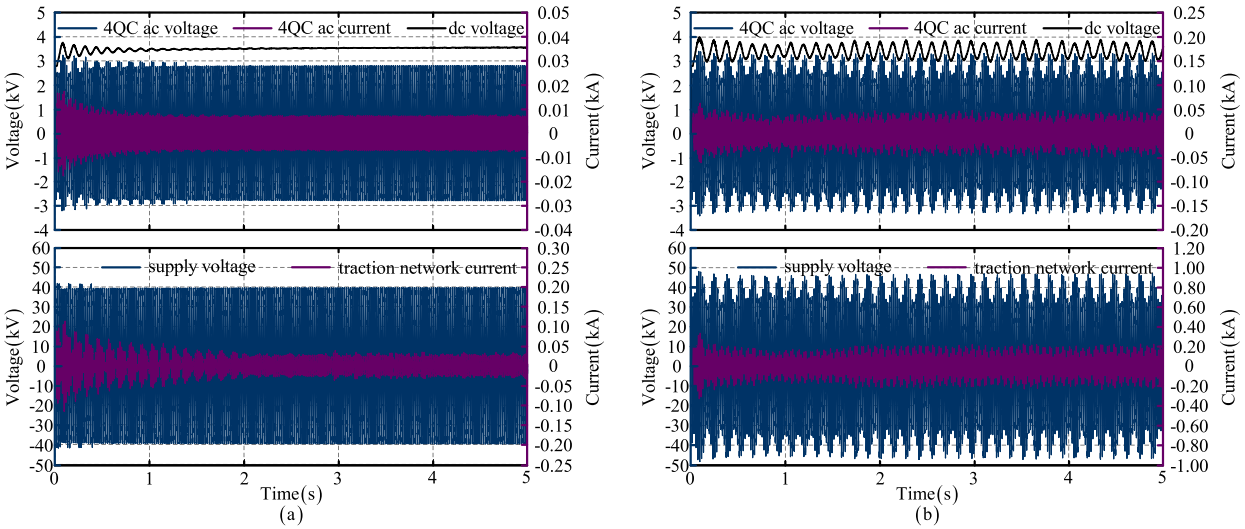

FIGURE 12. Waveforms of electrical quantities of the NTS with PI-based control. (a) 5 EMUs [stable, no LFO], (b) 6 EMUs [unstable, LFO] are put into operation.

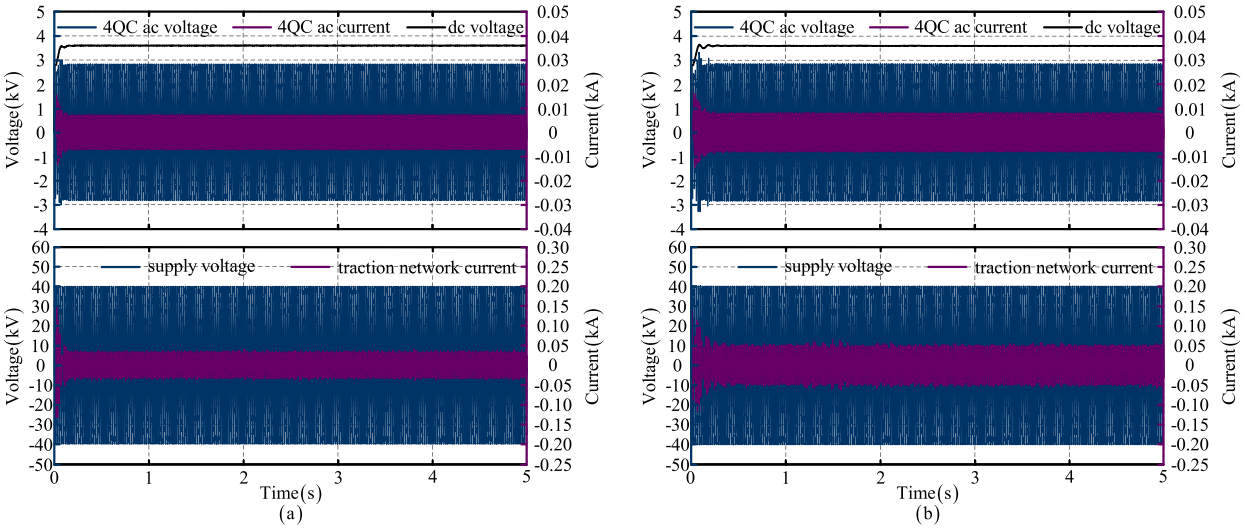

FIGURE 13. Waveforms of electrical quantities of the NTS with PBC-SMS control. (a) 6 EMUs [stable, no LFO], (b) 9 EMUs [stable, no LFO] are put into operation.

when 5 EMUs are working under the same supply, the ac and dc voltages of a 4QC as well as the traction network current (total line current of all the EMUs) show oscillations which are completely attenuated after 2 s. However, as shown in Fig. 12(b), LFO appears in the system when one more EMU is added (i.e. 6 EMUs). On the network side, the oscillation range of the supply voltage amplitude is 35-46 kV, and that of the traction network current is 86-225 A. On the 4QC side, the dc voltage fluctuates between 3010 V to 3892 V, showing a 7-7.3 Hz frequency. Owing to the reliability of the network parameters from the field test and the 4QC parameters introduced from [4], this set of simulation results are consistent to actual LFO phenomena of Section II-A as well as the stability analysis results given in Section II-C. This validates the feasibility and effectiveness of the modeling and stability analysis methods.

2) PROPOSED PBC-SMS CONTROLLER

The proposed PBC-SMS is tested in the NTS in order to validate its LFO suppression capability. For 6 EMUs, as shown in Fig. 13(a), all the voltages and currents on both network side and 4QC side are stable. In other words, the LFO is suppressed by replacing the conventional controller with the proposed one. Moreover, when increasing the EMU number to 9, the system remains stable as shown in Fig. 13(b). Due to the computational complexity of the off-line simulation, cases of more than 9 EMUs are not simulated. However, their performance is expected to match the analytical solutions of Section IV.

In conclusion, based on the parameters calculated from the field tested data, simulation tests validate that the PBC-SMS can effectively suppress the LFO and provides better steady-state and dynamic performance compared to more conventional methods.

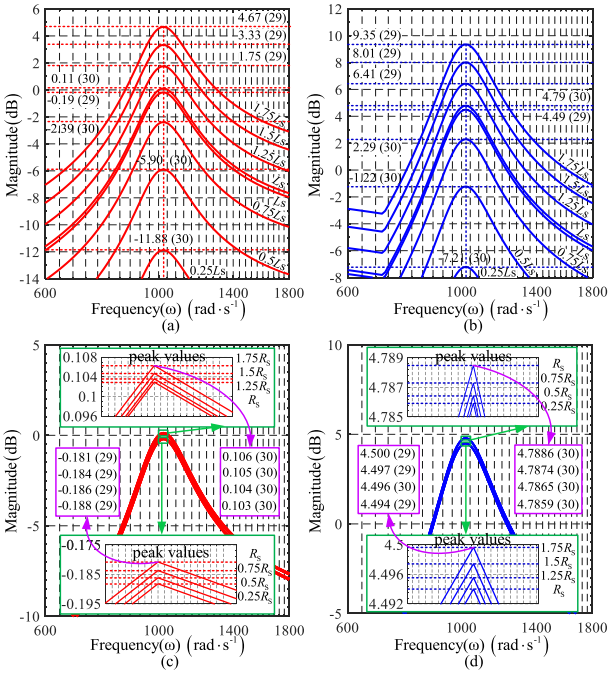

FIGURE 14. Stability analysis of the NTS with PBC-SMS when traction network parameters change. (a)/(b) 0.25 $L_S \rightarrow 1.75\ L_S$; (c)/(d) $0.25R_S \rightarrow 1.75R_S$. (In Figs. 14-17, the numbers in the brackets indicate the numbers of EMUs.)

VI. SENSITIVITY STUDY AND SUGGESTIONS

In an NTS there are three sets of parameters influencing the system stability: i) traction network parameters (R_S and L_S), ii) 4QC circuit parameters (r_L, L and C) and iii) control parameters (K_{IP}, K_{II}, K_{UP}, K_{UI} for PI control / k_1 (=k_2) and r_1 (=r_2) for PBC-SMS). The first forms the network impedance ($\boldsymbol{Z}_{Sdq}$), the latter two collectively form the multi-EMUs admittance ($\boldsymbol{Y}_{Ldq}$). Based on the G-sum norm criterion and modeling of Sections II and IV, parameters of values different from TABLE A are tested for investigating the parameter impact on the system stability. For simplicity, in the following analysis, the magnitude-frequency diagrams display the critical region around the peak values of the red and blue curves.

A. SENSITIVITY STUDY BASED ON PBC-SMS

A first set of parameter tests of the system with PBC-SMS are carried out considering 29 and 30 EMUs under the supply which is the critical condition from Section IV.

1) TRACTION NETWORK PARAMETERS

Keeping all other parameters constant, stability analysis results of varying L_S are given in Figs. 14(a) and (b). Comparing with Fig. 8(c), the system containing 30 EMUs becomes stable by decreasing the network inductance ($L_S \rightarrow 0.75L_S \rightarrow 0.5L_S \rightarrow 0.25L_S$). On the contrary, comparing with Fig. 8(b), the system with 29 EMUs becomes unstable by increasing the inductance ($L_S \rightarrow 1.25L_S \rightarrow 1.5L_S \rightarrow 1.75L_S$).

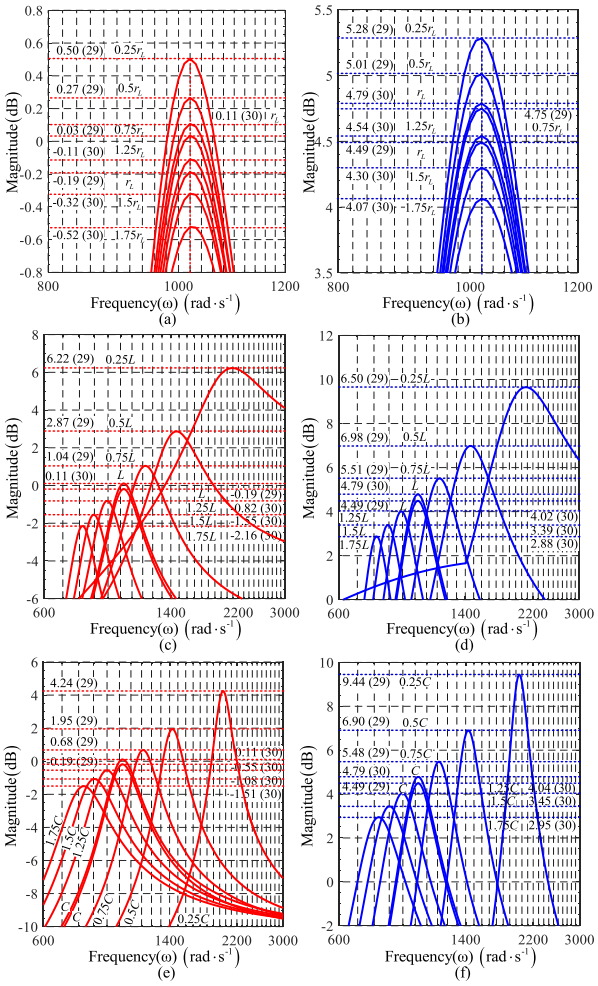

FIGURE 15. Stability analysis of the NTS with PBC-SMS when 4QC circuit parameters change. (a)/(b) 0.25 $r_L \rightarrow 1.75r_L$; (c)/(d) 0.25 $L \rightarrow 1.75\ L$; (e)/(f) 0.25 $C \rightarrow 1.75\ C$.

Similarly, the impact of R_S is then tested as shown in Figs. 14(c) and (d). Comparing them with Figs. 8(c) and (b), it is found that increasing R_S tends the system to instability, and inverse impact is obtained by decreasing R_S.

Comparing Figs. 14(a) and (b) with Figs. 14(c) and (d), one can see that L_S is the dominant network parameters for NTS stability.

2) 4QC CIRCUIT PARAMETERS

Comparing Fig. 15 with Figs. 8(b) and (c), it is found that the system: with 29 EMUs becomes unstable by decreasing any of r_L, L and C; with 30 EMUs becomes stable through increasing any of these parameters. In addition, among the three, L is the dominant parameter that affects the stability curves.

3) 4QC CONTROL PARAMETERS

Comparing Figs. 16(a) and (b) with Figs 8(b) and (c), it can be found that there is no significant change on maximum points of the curves when decreasing or increasing $k_1(= k_2)$. Therefore, the impact of k_1 and k_2 can be ignored.

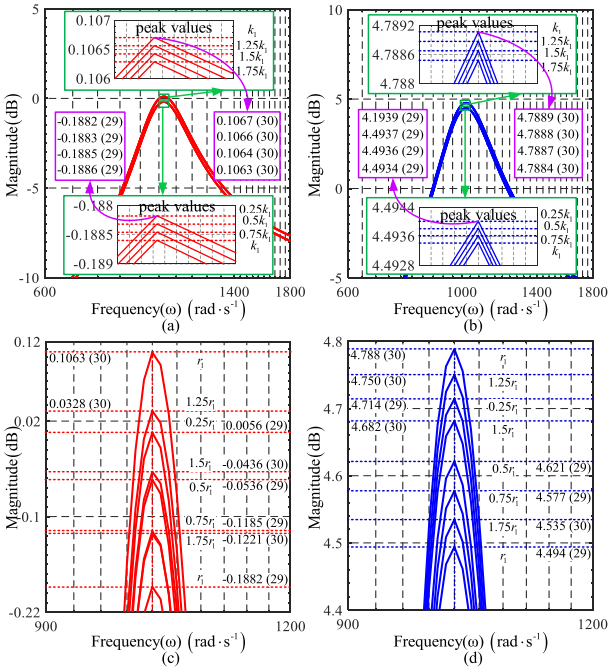

FIGURE 16. Stability analysis of the NTS with PBC-SMS when 4QC control parameters change. (a)/(b) 0.25 k_1(0.25k_2) → 1.75 k_1(1.75k_2); (c)/(d) 0.25r_1(0.25r_2) → 1.75 r_1(1.75 r_2).

In Fig. 16(c), increasing $r_1(=r_2)$ to $1.25r_1$, $1.5r_1$ and $1.75r_1$, the maximum point of the red curves decreases by 0.0735, 0.1499 and 0.2284 dB, respectively. In contrast, decreasing $r_1(=r_2)$ to $0.75r_1$, $0.5r_1$ and $0.25r_1$, the maximum point of the red curves in Fig. 16(c) increases by 0.0697, 0.1346 and 0.1938 dB, respectively. Therefore, r_1 and r_2 are the dominant impact factors, and decreasing them tends the NTS to instability. Although being of secondary concern, similar impact of the $r_1(=r_2)$ values on the blue curve is demonstrated in Fig. 16(d).

B. SENSITIVITY STUDY BASED ON PI

A second set of parameter tests based on conventional PI control are carried out considering 5 and 6 EMUs in the NTS which represents the critical condition from Section II. The results of network and 4QC circuit parameters are similar to the previous case and have been omitted. Relative curves of the variation of controller parameters are demonstrated in Fig. 17. Quantitative stability results are listed in TABLE 3. As shown in Fig. 17(a), increasing K_{IP} to $1.25K_{IP}$, $1.5K_{IP}$ and $1.75K_{IP}$, the maximum points of the red curves decrease by 0.97, 1.54 and 2.2 dB, respectively, enhancing the system stability. In contrast, decreasing K_{IP} to $0.75K_{IP}$, $0.5K_{IP}$ and $0.25K_{IP}$, the maximum points of the red curves increase by 0.96, 1.77 and 2.94 dB, respectively, destabilizing the system. Similar effect of K_{IP} on the blue curve is given in Fig. 17(b). Figs. 17(c)-(f) show that decreasing K_{II} or K_{UP} improves the system stability and inverse effect can obtained by increasing them. Figs. 17(g) and (h) show that the K_{UI} has little effect on the stability curves, thus can be ignored. Among them, K_{IP} is the dominant parameter impacting the NTS stability.

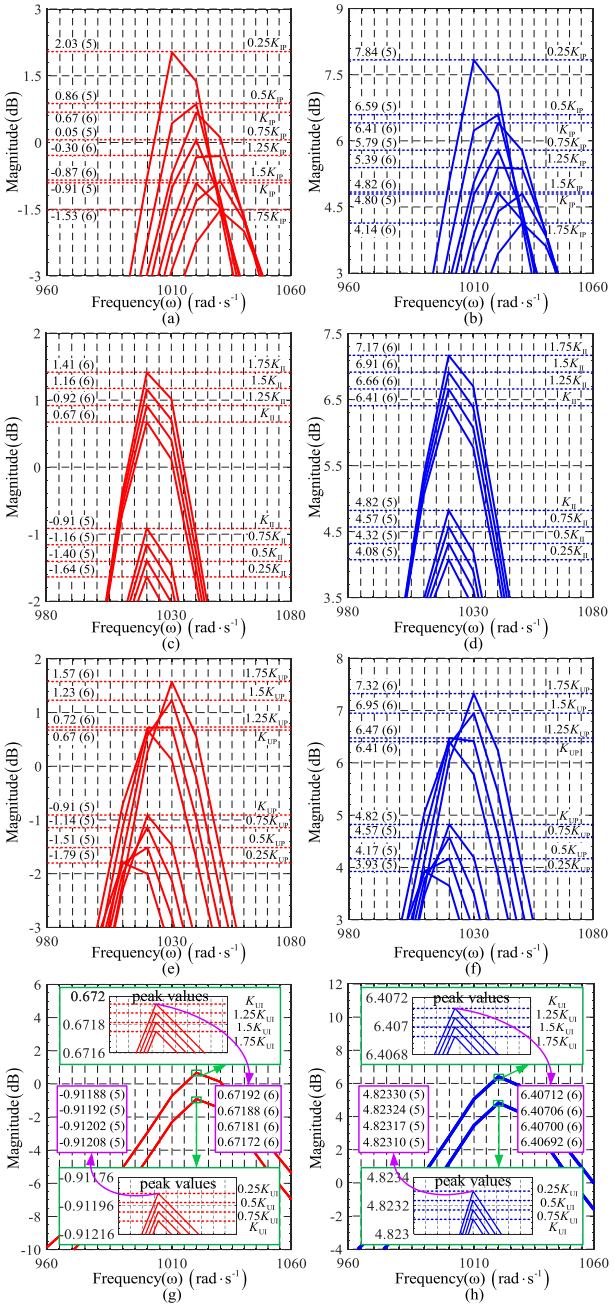

FIGURE 17. Stability analysis of the NTS with PI-based control when 4QC circuit parameters change. (a)/(b) 0.25 K_{IP} → 1.75 K_{IP}; (c)/(d)0.25 K_{II} → 1.75 K_{II}; (e)/(f)0.25 K_{UP} → 1.75 K_{UP}; (g)/(h)0.25 K_{UI} → 1.75 K_{UI}.

C. SUMMARY

Quantitative parameter sensitivity of the NTS stability for both the two 4QC control methods are summarized in TABLE 3. In summary: i) increasing the L_S will destabilize the NTS; ii) and the impact of R_S can be ignored in contrast to L_S; iii) the NTS stability can be enhanced by increasing any of the 4QC circuit parameters (r_L, L and C); iv) for conventional PI-based control, increasing K_{II} and K_{UP} or decreasing K_{IP} turns the system to instability; v) K_{UI} has less impact on NTS

TABLE 3. Correspondence between the NTS stability and different parameters.

Common parameters					Two control strategy									
Traction network		4QC circuit parameters			Control parameters of PI					Control parameters of PBC-SMS				
R_S (Ω)	L_S (H)	r_L (Ω)	L (H)	C (F)	K_{IP}	K_{II}	K_{UP}	K_{UI}	Stability	k_1	k_2	r_1 (Ω)	r_2 (Ω)	Stability
0.586	0.005↓	0.146	0.0054	0.009	0.86	7.5	1.9	0.1	↑	0.01	0.01	2.2	2.2	↑
	0.010↓								↑					↑
	0.015↓								↑					↑
	0.025↑								↓					↓
	0.030↑								↓					↓
	0.035↑								↓					↓
0.1465↓	0.02								-					-
0.2930↓									-					-
0.4395↓									-					-
0.7325↑									-					-
0.8790↑									-					-
1.0255↑									-					-
0.586	0.02	0.0365↓	0.0054	0.009	0.86	7.5	1.9	0.1	↓	0.01	0.01	2.2	2.2	↓
		0.0730↓							↓					↓
		0.1095↓							↓					↓
		0.1825↑							↑					↑
		0.2190↑							↑					↑
		0.2555↑							↑					↑
		0.146	0.00135↓	0.009					↓					↓
			0.00270↓						↓					↓
			0.00405↓						↓					↓
			0.00675↑						↑					↑
			0.00810↑						↑					↑
			0.00945↑						↑					↑
		0.146	0.0054	0.00225↓					↓					↓
				0.00450↓					↓					↓
				0.00675↓					↓					↓
				0.01125↑					↑					↑
				0.01350↑					↑					↑
				0.01575↑					↑					↑
0.586	0.02	0.146	0.0054	0.009	0.215↓	7.5	1.9	0.1	↓	0.0025↓	0.01	2.2	2.2	-
					0.430↓				↓	0.0050↓				-
					0.645↓				↓	0.0075↓				-
					1.075↑				↑	0.0125↑				-
					1.290↑				↑	0.0150↑				-
					1.505↑				↑	0.0175↑				-
					0.86	1.875↓	1.9	0.1	↑	0.01	0.0025↓	2.2	2.2	-
						3.750↓			↑		0.0050↓			-
						5.625↓			↑		0.0075↓			-
						9.375↑			↓		0.0125↑			-
						11.250↑			↓		0.0150↑			-
						13.125↑			↓		0.0175↑			-
					0.86	7.5	0.475↓	0.1	↑	0.01	0.01	0.55↓	2.2	↓
							0.950↓		↑			1.10↓		↓
							1.425↓		↑			1.65↓		↓
							2.375↑		↓			2.75↑		↑
							2.850↑		↓			3.30↑		↑
							3.325↑		↓			3.85↑		↑
					0.86	7.5	1.9	0.025↓	-	0.01	0.01	2.2	0.55↓	↓
								0.050↓	-				1.10↓	↓
								0.075↓	-				1.65↓	↓
								0.125↑	-				2.75↑	↑
								0.150↑	-				3.30↑	↑
								0.175↑	-				3.85↑	↑

Note: ↑ means the stability of the NTS is increased; - means the stability of the NTS does not change significantly; ↓ means the stability of the NTS is reduced.

stability than K_{II}, K_{UP} and K_{IP}; vi) for proposed PBC-SMS, increasing r_1 and r_2 will further improves the NTS stability, while k_1 and k_2 have few impact.

D. GUIDELINES FOR LFO SUPPRESSION

According to the sensitivity analysis of this section, four recommendations are made:

1) Increasing the number of 4QCs/EMUs essentially increases the total admittance $\boldsymbol{Y}_{\mathrm{Ldq}}$ of EMUs, which will lead to instability of the NTS. Thus, **limiting the number of EMUs** under the same supply section will reduce the possibility of LFOs.
2) The smaller the values of L_{S} and R_{S} are, the more stable the NTS will be. Moreover, L_{S} is the dominant network parameter. **Increasing the capacity of an ESS (e.g. transformer) is beneficial to LFO suppression**.
3) Larger values of r_L, L and C improve NTS stability; L is the dominant one among the three. To reduce LFO, it is suggested to **choose on-board transformers with large leakage impedance**.
4) According to sensitivity analysis of 4QC control parameters, appropriate selection and tuning of parameters will reduce the potential of LFOs. Therefore, **a design suggestion is to decrease K_{II}, K_{UP} or to increase K_{IP} of the PI controllers**. For the proposed PBC-SMS control, an increase of r_1 and r_2 has further LFO suppression effect.

VII. CONCLUSION

In this work, low-frequency oscillations, a typical issue in network-train system that affects the safe and stable operation of high-speed railways, is analyzed from the stability angle based on the G-sum norm criterion. A PBC-SMS method consisting of dc voltage SMS control and ac current PBC for EMU 4QC control is proposed for LFO suppression. The stability analysis illustrates that the proposed PBC-SMS provides superior LFO critical condition comparing to conventional PI-based control. Compared to conventional methods, the proposed PBC-SMS provides better steady-state and dynamic performance and superior LFO suppression capability. The proposed controllers are validated through extensive simulation tests developed using field data measurements for the models. A sensitivity analysis considering the traction network, 4QC circuit and controller parameters of the NTS is carried out, suggesting a number of guidelines for LFO suppression.

Note that the controller parameters are dependent to the EMU circuit parameters. However, the proposed control method is not limited to a single EMU model. It can be readily extended to another system with specific circuit parameters by simply re-tuning the controller parameters. Further work in the area can consider adaptive techniques to improve the flexibility of the proposed PBC-SMS method across multiple EMU models.

APPENDIX A

Electrical parameters used in the stability analysis, simulation verification of this work are listed in TABLE 4, in where the network parameters are estimated based on the field tested data of the LFO incident of Section II-A; the 4QC circuit is introduced from [4], and PI controller parameters are determined through simulation; the PBC-SMS parameters are obtained by simulation tuning.

TABLE 4. Parameters of the NTS.

Parameters		Description	Values
Traction network	e_{S}	The output voltage of ESS	27500 V
	u_{S}	The network-side voltage of the 4QCs	25000 V
	$u_{\mathrm{S}}^{(2)}$	The secondary voltage of the 4QCs	1770 V
	R_{S}	Equivalent resistance of the traction network	0.586 Ω
	L_{S}	Equivalent inductance of the traction network	0.02 H
4QC circuit	L	Equivalent inductance of on-board transformer	0.0054 F
	r_L	Equivalent resistance of on-board transformer	0.146 Ω
	C	The dc-link capacitor	0.009 F
	R_{o}	The load equivalent resistance	662 Ω
	u_{dc}	The 4QC dc voltage	3600 V
PI	K_{UP}	Proportional coefficient of the voltage controller	1.9
	K_{UI}	Integral coefficient of the voltage controller	0.1
	K_{IP}	Proportional coefficient of the current controller	0.86
	K_{II}	Integral coefficient of the current controller	7.5
PBC-SMS	k_1	The gains of PBC-SMS controller	0.01
	k_2	The gains of PBC-SMS controller	0.01
	r_1	The injection damping	2.2 Ω
	r_2	The injection damping	2.2 Ω

REFERENCES

[1] W. Song, J. Ma, L. Zhou, and X. Feng, "Deadbeat predictive power control of single-phase three-level neutral-point-clamped converters using space-vector modulation for electric railway traction," *IEEE Trans. Power Electron.*, vol. 31, no. 1, pp. 721–732, Jan. 2016.
[2] K. Song, G. Konstantinou, W. Mingli, P. Acuna, R. P. Aguilera, and V. G. Agelidis, "Windowed SHE-PWM of interleaved four-quadrant converters for resonance suppression in traction power supply systems," *IEEE Trans. Power Electron.*, vol. 32, no. 10, pp. 7870–7881, Oct. 2017.
[3] H. Wang and M. Wu, "Review of low-frequency oscillation in electric railways," *Trans. China Electro Tech. Soc.*, vol. 30, pp. 70–78, Sep. 2015.
[4] H. Wang, W. Mingli, and J. Sun, "Analysis of low-frequency oscillation in electric railways based on small-signal modeling of vehicle-grid system in dq frame," *IEEE Trans. Power Electron.*, vol. 30, no. 9, pp. 5318–5330, Sep. 2015.
[5] S. Danielsen, M. Molinas, T. Toftevaag, and O. B. Fosso, "Constant power load characteristic's influence on the low-frequency interaction between advanced electrical rail vehicle and railway traction power supply with rotary converters," in *Proc. Mod. Electr. Traction*, 2009, pp. 1–6.
[6] E. Mollerstedt and B. Bernhardsson, "Out of control because of harmonics-an analysis of the harmonic response of an inverter locomotive," *IEEE Control Syst. Mag.*, vol. 20, no. 4, pp. 70–81, Aug. 2000.
[7] Q. Li, "Vehicle-grid electrical matching in electrified railways," *Electr. Railway*, vol. 5, no. 12, pp. 13–16, 2014.
[8] Z. Liu, G. Zhang, and Y. Liao, "Stability research of high-speed railway EMUs and traction network cascade system considering impedance matching," *IEEE Trans. Ind. Appl.*, vol. 52, no. 5, pp. 4315–4326, Sep. 2016.
[9] Y. Zhou, H. Hu, X. Yang, and Z. He, "Analysis of low-frequency oscillation in train-traction network coupled system of electrified railway," *Proc. CSEE*, vol. 37, pp. 72–80, Sep. 2017.
[10] Y. Liao, Z. Liu, G. Zhang, and C. Xiang, "Vehicle-grid system stability analysis considering impedance specification based on norm criterion," in *Proc. IEEE Transp. Electrific. Conf. Expo, Asia–Pacific (ITEC Asia–Pacific)*, Jun. 2016, pp. 118–123.
[11] Y. Liao, Z. Liu, G. Zhang, and C. Xiang, "Vehicle-grid system modeling and stability analysis with forbidden region-based criterion," *IEEE Trans. Power Electron.*, vol. 32, no. 5, pp. 3499–3512, May 2017.
[12] K. Jiang, C. Zhang, and X. Ge, "Low-frequency oscillation analysis of the train-grid system based on an improved forbidden-region criterion," *IEEE Trans. Ind. Appl.*, vol. 54, no. 5, pp. 5064–5073, Sep. 2018.
[13] G. Zhang, Z. Liu, S. Yao, Y. Liao, and C. Xiang, "Suppression of low-frequency oscillation in traction network of high-speed railway based on auto-disturbance rejection control," *IEEE Trans. Transp. Electrific.*, vol. 2, no. 2, pp. 244–255, Jun. 2016.

[14] J. Xu, H. Cheng, W. Huang, Y. Liu, Z. Chen, and B. An, "A novel approach based on self-adaptive auto disturbance rejection proportional integral controller to suppress low frequency oscillation of high-speed railway electric multiple units-traction network coupling system," *Proc. CSEE*, vol. 37, no. 9, pp. 72–80, Jul. 2017.

[15] Z. Liu, C. Xiang, Y. Wang, Y. Liao, and G. Zhang, "A model-based predictive direct power control for traction line-side converter in high-speed railway," *IEEE Trans. Ind. Appl.*, vol. 53, no. 5, pp. 4934–4943, Sep. 2017.

[16] Z. Liu, Y. Wang, S. Liu, Z. Li, H. Zhang, and Z. Zhang, "An approach to suppress low-frequency oscillation by combining extended state observer with model predictive control of EMUs rectifier," *IEEE Trans. Power Electron.*, vol. 34, no. 10, pp. 10282–10297, Oct. 2019, doi: 10.1109/TPEL.2019.2893491.

[17] Z. Geng, Z. Liu, X. Hu, and J. Liu, "Low-frequency oscillation suppression of the vehicle–grid system in high-speed railways based on H_∞ control," *Energies*, vol. 11, no. 6, p. 1594, Jun. 2018.

[18] Z. Liu, Z. Geng, and X. Hu, "An approach to suppress low frequency oscillation in the traction network of high-speed railway using passivity-based control," *IEEE Trans. Power Syst.*, vol. 33, no. 4, pp. 3909–3918, Jul. 2018.

[19] Z. Liu, Z. Geng, S. Wu, X. Hu, and Z. Zhang, "A passivity-based control of Euler–Lagrange model for suppressing voltage low-frequency oscillation in high-speed railway," *IEEE Trans. Ind. Informat.*, vol. 15, no. 10, pp. 5551–5560, Oct. 2019, doi: 10.1109/TII.2019.2903103.

[20] S. Liu, Z. Liu, Y. Wang, and Z. Geng, "A novel approach based on SMC to traction network voltage low frequency oscillation suppression research," *Power Syst. Technol.*, vol. 42, no. 9, pp. 2999–3006, Sep. 2018.

[21] W. Wang and Z. Gao, "A comparison study of advanced state observer design techniques," in *Proc. Annu. Amer. Control Conf. (ACC)*, 2003, pp. 475–4754.

[22] C. Xin, "An equivalent circuit derivation method of AT power supply system," *Electr. Railway*, vol. 35, no. 1, pp. 17–20, 1999.

[23] M. Wu, "Uniform chain circuit model for traction networks of electric railways," *Proc. CSEE*, vol. 30, no. 28, pp. 52–58, Oct. 2010.

[24] F. Wang, "Generalized method of symmetrical components and its applications," *J. Southwest Jiaotong Univ.*, vol. 4, no. 1, pp. 1–11, 1981.

[25] F. Liu, J. Liu, H. Zhang, H. Zhang, D. Xue, and Z. Liu, "G-norm and sum-norm based stability criterion for three-phase AC cascade systems," *Proc. CSEE*, vol. 34, no. 24, pp. 4092–4100, Aug. 2014.

[26] L. Fangcheng, L. Jinjun, Z. Haodong, X. Danhong, H. S. Ul, and Z. Linyuan, "Modified norm type stability criterion for cascade AC system," in *Proc. IEEE Energy Convers. Congr. Expo.*, Sep. 2013, pp. 442–447.

[27] M. Belkhayat, "Stability criteria for AC power systems with regulated loads," Ph.D. dissertation, Purdue Univ., West Lafayette, IN, USA, 1997.

[28] R. Burgos, D. Boroyevich, F. Wang, K. Karimi, and G. Francis, "On the AC stability of high power factor three-phase rectifiers," in *Proc. IEEE Energy Convers. Congr. Expo.*, Sep. 2010, pp. 2047–2054.

[29] R. Burgos, D. Boroyevich, F. Wang, K. Karimi, and G. Francis, "AC stability of high power factor multi-pulse rectifiers," in *Proc. IEEE Energy Convers. Congr. Expo.*, Sep. 2011, pp. 3758–3765.

[30] M. Wu and H. Wang, "The test of traction power blocking of CRH5 EMU caused by the voltage oscillation," Beijing Jiaotong Univ., Beijing, China, Tech. Rep. E11L00040, Sep. 2010.

[31] H. Wang and M. Wu, "The measurement and analysis of the low frequency oscillation in traction power supply system caused by the EMU," in *Proc. 27th Chin. Univ. Symp. Power Electr. Syst. Autom.*, Qinhuangdao, China, 2011, p. 1.

[32] D. Frugier and P. Ladoux, "Voltage disturbances on 25 kV-50 Hz railway lines-modelling method and analysis," in *Proc. Int. Symp. IEEE Power Electron. Electr. Drives Autom. Motion (SPEEDAM)*, Jun. 2010, pp. 1080–1085.

[33] C. Heising, M. Oettmeier, R. Bartelt, V. Staudt, and A. Steimel, "Single-phase 50 kW 16.7 Hz PI-controlled four-quadrant line-side converter lab model fed by rotary converter," in *Proc. 6th Int. Conf. Workshop Compat. Power Electron.*, Badajoz, Spain, May 2009, pp. 232–239.

[34] B. Wen, D. Boroyevich, R. Burgos, P. Mattavelli, and Z. Shen, "Analysis of D-Q small-signal impedance of grid-tied inverters," *IEEE Trans. Power Electron.*, vol. 31, no. 1, pp. 675–687, Jan. 2016.

[35] J. Silva, "Sliding-mode control of boost-type unity-power-factor PWM rectifiers," *IEEE Trans. Ind. Electron.*, vol. 46, no. 3, pp. 594–603, Jun. 1999.

[36] K. Huang, W. Wang, and X. Wang, "Modeling and simulation of PWM converters based on sliding-mode control," *Power Syst. Technol.*, vol. 33, no. 8, pp. 18–23, Apr. 2009.

[37] J. Li, X. Lv, B. Zhao, Y. Zhang, Q. Zhang, and J. Wang, "Research on passivity based control strategy of power conversion system used in the energy storage system," *IET Power Electron.*, vol. 12, no. 3, pp. 392–399, Mar. 2019.

SHAOBING YANG (Member, IEEE) received the B.S. degree in electrical engineering from Shanghai Jiaotong University, in 1995, and the M.S. and Ph.D. degrees in electrical engineering from Beijing Jiaotong University, in 2009 and 2016, respectively.

He is currently an Associate Professor with the School of Electrical Engineering, Beijing Jiaotong University. His current research areas include power system simulation, load modeling, demand side management, electric power quality, and load forecasting for electric vehicles.

YINGCHEN WANG was born in Anhui, China, in January 1994. He received the B.Sc. degree in electrical engineering and its automation from Lanzhou Jiaotong University, Lanzhou, China, in 2018. He is currently pursuing the M.Sc. degree in electrical engineering with Beijing Jiaotong University, Beijing, China.

His research interests include the stability analysis of network-train system in high-speed railways and harmonic impedance frequency characteristic of traction power supply systems.

KEJIAN SONG (Member, IEEE) was born in Hunan, China. He received the B.Sc. degree in electrical engineering from Shaoyang University, Shaoyang, China, in 2010, the M.Sc. and Ph.D. degrees in electrical engineering from Beijing Jiaotong University (BJTU), Beijing, China, in 2012 and 2017, respectively. From 2014 to 2015, he was with the Australia Energy Research Institute, University of New South Wales (UNSW), Sydney, Australia, as an Exchanged Ph.D. Student, sponsored by China Scholarship Council.

From 2017 to 2019, he was a Postdoctoral Researcher with BJTU. He is currently an Associate Professor with the School of Electrical Engineering, BJTU. His research interests include modulation methods and control strategies for traction converters and electric power quality of traction power supply systems.

MINGLI WU (Member, IEEE) was born in Hebei, China, in November 1971. He received the B.Sc. and M.Sc. degrees in electrical engineering from Southwest Jiaotong University, Chengdu, China, in 1993 and 1996, respectively, and the Ph.D. degree in electrical engineering from Beijing Jiaotong University (BJTU), Beijing, China, in 2006.

Since 2008, he has been a Professor with the School of Electrical Engineering, BJTU. His research interests include power supply for electric railways, digital simulation of power system, and electric power quality.

GEORGIOS KONSTANTINOU (Senior Member, IEEE) received the B.Eng. degree in electrical and computer engineering from the Aristotle University of Thessaloniki, Thessaloniki, Greece, in 2007, and the Ph.D. degree in electrical engineering from UNSW Sydney (The University of New South Wales), Australia, in 2012.

From 2012 to 2015, he was a Research Associate at UNSW. He is currently a Senior Lecturer with the School of Electrical Engineering and Telecommunications, UNSW Sydney, and an Australian Research Council (ARC) Early Career Research Fellow. His main research interests include multilevel converters, power electronics in HVDC, renewable energy, and energy storage applications. He is an Associate Editor of the IEEE TRANSACTIONS ON POWER ELECTRONICS and *IET Power Electronics*.